eLife

Reviewed Preprint
v2 • January 3, 2025
Revised by authors

Reviewed Preprint
v1 • January 19, 2024

Cancer Biology

Formation of malignant, metastatic small cell lung cancers through overproduction of cMYC protein in TP53 and RB1 depleted pulmonary neuroendocrine cells derived from human embryonic stem cells

Huanhuan Joyce Chen, Eric E Gardner, Yajas Shah, Kui Zhang, Abhimanyu Thakur, Chen Zhang, Olivier Elemento, Harold Varmus

Meyer Cancer Center, Weill Cornell Medicine, New York, USA. • The Pritzker School of Molecular Engineering, The University of Chicago, Chicago, USA. • The Ben May Department for Cancer Research, The University of Chicago, Chicago, USA • Caryl and Israel Englander Institute for Precision Medicine, Weill Cornell Medicine, New York, USA. • Department of Pathology and Laboratory Medicine, Weill Cornell Medicine, New York, USA.

eLife Assessment

Given a great need for novel human model systems to study small cell lung cancer (SCLC), the authors describe an **important** pre-clinical model with broad potential for the study of how genetic perturbations or drug treatments alter SCLC tumor growth, metastasis, and response to therapy. For the major finding, the authors provide **convincing** evidence that RB/TP53 suppression coupled with MYC overexpression in an ES cell-derived model system results in aggressive and metastatic SCLC. However, the impact of the work would have been increased with the inclusion of a broader set of genetic perturbations, such as over-expression of MYCL, to better model major SCLC phenotypes. The new model described will be of significant interest to researchers studying lung cancer.

https://doi.org/10.7554/eLife.93170.2.sa3

Abstract

We recently described our initial efforts to develop a model for small cell lung cancer (SCLC) derived from human embryonic stem cells (hESCs) that were differentiated to form pulmonary neuroendocrine cells (PNECs), a putative cell of origin for neuroendocrine-positive SCLC. Although reduced expression of the tumor suppressor genes *TP53* and *RB1* allowed the induced PNECs to form subcutaneous growths in immune-deficient mice, the tumors did not display the aggressive characteristics of SCLC seen in human patients. Here we report that the additional, doxycycline-regulated expression of a transgene encoding wild-type or mutant cMYC protein promotes rapid growth, invasion, and metastasis of these hESC-

derived cells after injection into the renal capsule. Similar to others, we find that the addition of cMYC encourages the formation of the SCLC-N subtype, marked by high levels of *NEUROD1* RNA. Using paired primary and metastatic samples for RNA sequencing, we observe that the subtype of SCLC does not change upon metastatic spread and that production of NEUROD1 is maintained. We also describe histological features of these malignant, SCLC-like tumors derived from hESCs and discuss potential uses of this model in efforts to control and better understand this recalcitrant neoplasm.

Introduction

From the earliest days of cancer research, attempts to understand the mechanisms of carcinogenesis have depended on experimental models to circumvent the ethical obstacles to performing experiments in human subjects. Such model systems have ranged from normal and cancerous human cells grown in animals or in cell culture to the generation or manipulation of cancers arising from normal cells in whole animals. The success of such approaches is often measured by the similarities of model systems to the observed traits of cancers that have arisen naturally in human subjects. But the utility of certain model systems can also be appraised by evaluation of the information that emerges from them, even when the models lack a clear relationship to any specific type of human cancer. The transformation of chicken embryo fibroblasts by Rous sarcoma virus or the induction of leukemias with various murine leukemia viruses exemplify models that lack verisimilitude but nevertheless have revealed major features of carcinogenesis (1).

A common complaint about many models of cancer is that the transformation of a normal cell to a malignant cell occurs in non-human cells. Efforts to transform human cells are often limited by the difficulties of growing human cells in culture and uncertainty about the developmental stage of a given cell lineage at which transformation generally occurs. Techniques for generating, propagating, and differentiating human stem cells - either tissue-specific stem cells or pluripotent stem cells - have raised the possibility of studying carcinogenesis in a wide variety of human cell lineages, as initially demonstrated for gliomas derived from induced human pluripotent stem cells (iPSCs) (2).

We have recently attempted to study the mechanisms by which small cell lung cancer (SCLC) arises in human lung cells by efficiently differentiating human embryonic stem cells (hESCs) (3, 4) into mature lung epithelial cells, including the likely precursor of SCLC (pulmonary neuroendocrine cells [PNECs]) and then simulating loss of function of the tumor suppressor genes *TP53* and *RB1*, tumor suppressors commonly lost in human SCLC (5). PNEC-like cells that have lost the function of these two tumor suppressor genes, by expression of short hairpin RNAs (shRNAs) specific for *RB1* and *TP53*, can form tumors subcutaneously in immunodeficient mice; however, these tumors grow slowly and do not invade or metastasize, standing in contrast to what is known about the clinical presentation and behavior of SCLC (6). Thus, the original hESC-derived SCLC models we generated appeared to be benign growths that do not resemble SCLCs functionally, limiting their utility as models for aggressive human SCLC.

Our earlier findings are consistent with the idea that full transformation of PNECs to form malignant SCLC requires additional changes beyond restricted expression of the tumor suppressor genes *RB1* and *TP53*, such as heightened expression of a proto-oncogene in the *MYC* family (7, 8). In an attempt to show that we can generate more aggressive, SCLC-like tumors from PNECs derived from hESCs, we have added efficiently transcribed *cMYC* oncogenes to cells in which expression of *TP53* and *RB1* are inhibited by shRNAs. When these cells were then injected into renal capsules of immunodeficient mice, some produced rapidly expanding tumors that invaded locally and sometimes formed metastatic growths, mostly in the liver.

In this report, we describe morphological and transcriptional features of these tumors and discuss how the addition of putative drivers of SCLCs can be used to study the mechanism of carcinogenesis and to test candidate therapies for this “recalcitrant” cancer.

Materials and Methods

Generation of lung cells, including PNECs, from hESCs

Protocols for maintenance of hESCs and generation of pulmonary neuroendocrine cells (PNECs), and other lung cells were modified from previous studies (3-5). Two hESC lines, RUES2 (Rockefeller University Embryonic Stem Cell Line 2, NIH approval number NIH hESC-09-0013, Registration number 0013; passage 7-10) and ES02 (HES2, NIH registry, WiCell Research Insititute, Inc. passage 3-7) were cultured and maintained in an undifferentiated state on irradiated mouse embryonic fibroblasts (Global Stem, cat. no. GSC-6001G). All cells were purchased from ATCC or WiCell in the past 3 years and tests for mycoplasma were negative. The hESC lines were regularly checked for chromosome abnormalities and maintained with normal chromosome numbers. All embryonic stem cell studies were approved by the Institutional Review Board (IRB) at the University of Chicago, or by the Tri-Institutional ESCRO committee under protocols 2016-01-002 and 2017-10-004 (Weill Cornell Medicine, Memorial Sloan Kettering Cancer Center, and Rockefeller University).

hESC differentiation into endoderm was performed in serum-free differentiation (SFD) media of DMEM/F12 (3:1) (Life Technologies) supplemented with N2 (Life Technologies), B27 (Life Technologies), ascorbic acid (50 μg/ml, Sigma), Glutamax (2 mM, Life Technologies), monothioglycerol (0.4 μM, Sigma), 0.05% bovine serum albumin (BSA) (Life Technologies) at 37C in a 5% CO_2 / 5% O_2 / 90% N_2 environment. hESCs were treated with Accutase (Stemcell technology) and plated onto low attachment 6-well plates (Corning Incorporated, Tewksbury MA), resuspended in endoderm induction media containing Y-27632 (10 μM), human BMP4 (0.5 ng/ml), human bFGF, (2.5 ng/ml), and human Activin A (100 ng/ml) for 72 – 84 hours (hrs) dependent on the formation rates of endoderm cells. On day 3 or 3.5, the embryoid bodies were dissociated into single cells using 0.05% Trypsin/0.02% EDTA and plated onto fibronectin-coated (Sigma), 24-well tissue culture plates (~100,000– 150,000 cells/well). For induction of anterior foregut endoderm, the endoderm cells were cultured in SFD medium supplemented with 1.5 μM Dorsomorphin dihydrochloride and 10 μM SB431542 for 36-48 hrs, and then switched to 36-48 hrs of 10 μM SB431542 and 1 μM IWP2 treatment.

For induction of early-stage lung progenitor cells (days 6–15), the resulting anterior foregut endoderm was treated with CHIR99021 (3 μM), human FGF10 (10 ng/ml), human FGF7 (10 ng/ml), human BMP4 (10 ng/ml) and all-*trans* retinoic acid (ATRA; 50nM) in SFD medium for 8–10d. Day 10–15 cultures were maintained in a 5% CO2/air environment. On days 15 and 16, the lung field progenitor cells were re-plated after brief one-minute trypsinization onto fibronectin-coated plates, in the presence of SFD containing either a combination of five factors: CHIR99021 (3 μM), human FGF10 (10 ng/ml), human FGF7 (10 ng/ml), human BMP4 (10 ng/ml), and ATRA (50 nM), or three factors: CHIR99021 (3 μM), human FGF10 (10 ng/ml), and human FGF7 (10 ng/ml) for days 14-16. Day 16–25 cultures of late-stage lung progenitor cells were maintained in SFD media containing CHIR99021 (3 μM), human FGF10 (10 ng/ml), and human FGF7 (10 ng/ml) in a 5% CO2 / air environment.

For differentiation of mature lung cells (days 25–55), cultures were re-plated after brief trypsinization onto 3.3% matrigel coated 24-well plates in SFD media containing maturation components CHIR99021 (3 μM), human FGF10 (10 ng/ml), human FGF7 (10 ng/ml), and DCI (50 nM Dexamethasone, 0.1 mM 8-bromo-cAMP and 0.1 mM IBMX (3,7-dihydro-1-methyl-3-(2-methylpropyl)-1*H*-purine-2,6-dione). DAPT (10 μM) was added to the maturation media for

induction of PNECs. All growth factors and most small molecules used for hESC differentiation were purchased from R&D Systems. ATRA, 8-bromo-cAMP, IBMX and DAPT were purchased from Sigma-Aldrich.

Lentivirus transduction of hESCs

HSC lines were constructed to contain DOX-inducible cassettes encoding shRNAs specific for the *TP53* and *RB1* tumor suppressor genes (RP cells) and RP cells containing DOX-inducible cassettes encoding wildtype human cMYC or a stable, mutant version of cMYC (T58A), to generate RPM and RPM (T58A) cells. The lentiviral vector expressing tetracycline (TET)-inducible shRNA against human P53 was purchased from Gentarget. Inc. (cat# LVP-343-RB-PBS). The lentiviral vectors expressing TET-inducible shRNAs against human *RB1* construct ("pSLIK sh human Rb 1534 hyg" was a gift from Julien Sage; plasmid # 31500) (9), TET-inducible wild type cMYC (FUW-tetO-hMYC was a gift from Rudolf Jaenisch; plasmid # 20723) or mutant cMYC (T58A) tagged at the N-terminus with three copies of a hemagglutinin tag (3X-HA) (pLV-tetO-myc T58A was a gift from Konrad Hochedlinger; plasmid # 19763) were obtained from Addgene and sequence verified prior to use. The shRNA target sequences are as follows: RB1 #1: 5'-GGACATGTGAACTTATATA-3', RB1 #2: 5'-GAACGATTATCCATTCAAA-3', p53: 5'-CACCATCCACTACAACTACAT-3'.

To generate lentiviral particles, the above plasmids were transfected into HEK293T cells with the PC-Pack2 lentiviral packaging mix (Cellecta, Inc.), according to the manufacturer's protocol. High titer viral particles were used to transduce hESCs in serum-free conditions and antibiotic selection of transduced hESCs was performed without MEF feeder cells, using mTeSR1 stem cell media (Stemcell Tech. Inc.). The efficiency of *RB1* or *P53* knockdown and production of cMYC or cMYC (T58A) were determined by Western Blot after antibiotic selection using the following antibodies: anti-RB1 (Cell Signaling, clone 4H1, Cat# 9309), anti-P53 (Santa Cruz, clone DO-1, Cat# Sc-126), anti-MYC (Cell Signaling, clone D84C12, Cat# 5605), anti-HA (Cell Signaling, clone 6E2, Cat#2367), and anti-GAPDH (Cell Signaling, clone 14C10, Cat# 2118). All antibodies for Western Blot were used at a 1:500 working dilution.

Immunohistochemistry

Living cells in culture were directly fixed in 4% paraformaldehyde for 25 min, followed with 15 min permeabilization in 1% Triton X-100. Histology on tissues from mice was performed on paraffin-embedded or frozen sections from xenografted tumors and corresponding normal tissues, as previously described (10). Tissues were either fixed overnight in 10% buffered formalin and transferred to 70% ethanol, followed by paraffin embedding, or snap frozen in O.C.T medium (Fisher Scientific, Pittsburgh, PA) and fixed in 10% buffered formalin, followed by paraffin embedding. For immunofluorescence, cells or tissue sections were immunostained with antibodies and counterstained with 4,6-diamidino-2-phenylindole (DAPI). Adjacent sections stained with H&E were used for comparison.

Antibodies used for immunostaining or western blot experiments are as follows: anti-CGRP (Sigma, Clone CD8, Cat# c9487), anti-ASCL1 (Sigma, clone 2D9, Cat# SAB1403577), anti-NCAM1/CD56 (R&D systems, cat# AF2408), anti-Ki67 (Cell Signaling, clone D2H10, Cat# 9027, anti-MYC (Abcam, clone Y69, Cat# ab32072), and anti-NEUROD1 (Sigma-Aldrich, clone 3H8, Cat# WH004760M1). All antibodies were used at a 1:150 working dilution.

Fluorescent activated cell sorting (FACS)

FACS to detect definitive endoderm cells was performed using APC anti-c-KIT (Invitrogen, Cat# CD11705), PE anti-human CXCR4 (Biolegend, Clone 12G5, Cat# 306506) and APC anti-EpCAM (Invitrogen, Clone G8.8, Cat# 17-5791-80) at 1:100 dilution. Cells were incubated with primary antibodies for 30 minutes at 4°C, then washed and suspended in 0.1% BSA/PBS buffer. PE and APC filters were then used to detect cells double positive for KIT and CXCR4, or EpCAM and CXCR4 by

signal intensity gating. FACS with anti-CGRP antibody (Abcam, clone 4902, Cat# ab81887) was used to detect CGRP+ cells. Cells were first incubated with anti-human CGRP antibody for 30 minutes at room temperature followed with incubation (1:1000) of secondary antibody conjugated with R-phycoerythrin (PE) for 30 min at room temperature. Then cells were washed and suspended in 0.1% BSA/PBS buffer. PE filter was then used to separate cells into CGRP+ and CGRP-sub-groups by signal intensity gating. Negative controls stained with isotype controls were performed with sample measurements. Cells were sorted on a BD FACSAria II and data were analyzed in FlowJo.

Xenograft formation

0.3-0.5 × 10^6 hESC-derived lung cells or PNECs (at day 55 with or without 30 days of prior exposure to 10 μM DAPT alone or to 10 μM DAPT and 1 μM doxycycline to reduce *P53* and *RB1*, and also induce *MYC* expression) were injected subcutaneously or under the renal capsule of 6-8 weeks old, female NOD.Cg-*Prkdc*^{scid} *Il2rg*^{tm1WjI}/SzJ (NSG) mice (Jackson Laboratory, Bar Harbor, Maine) (11). Doxycycline diet began the day after injection (Teklad; 625ppm); tumor development was monitored at least 2-3 times weekly. When animals became moribund or tumor size reached protocol limitations, mice were sacrificed, necropsy performed, and tumors harvested for further histological or molecular study.

Single cell sequencing and data analysis

Single-cell capture, reverse transcription, cell lysis, and library preparation were carried out by the WCM Epigenomics Core Facility using Chromium Single Cell 3' v3 kits according to the manufacturer's protocol (10x Genomics, USA). Single cell suspenions of RUES2-dervied RPM and RPM (T58A) day 50 cultures were prepared by incubating wells in 0.05% Trypsin/0.02% EDTA for 10-15 min. Digestions were then quenched with excess 0.1% BSA/PBS buffer and passed through 40μm mesh strainer. EGFP+ singlets were sorted at the WCM Flow Cytometry Core Facility on a BD Influx or Sony MA900 cell sorter. Each RUES2-dervied RPM and RPM(T58A) day 50 culture pools were isolated from 3 wells of a 12-well plate across two biological replicates, targeting ~50,000 viable, EGFP+ viable cells per replicate. Cell counts were then adjusted to 6000-9000 cells/50uL in PBS by Trypan Blue exclusion to achieve an estimated capture of 4000-5000 cells. Sequencing was performed by the WCM Genomics Resources Core Facility on a HiSeq 2500 (Illumina, paired-end protocol with 26 base pairs for read 1 and 98 bases for read 2). Single cell RNA sequencing from RP cultures were obtained from previous experiments (5). Transcript abundance was quantified by mapping sequencing reads to a custom human transcriptome reference (GENCODE v42, hg38) that included EGFP and was performed using simpleaf/alevin-fry (12).

Single-cell analyses, including quality filtering, integration, clustering, differential gene expression and reduced-dimensionality visualization, were performed using the Seurat package in R as described in the package SCTransform tutorial (Version 4.3.0) (13). Briefly, cells to be included in the analysis were required to have at least 4000 and at most 45000 unique molecular identifiers (UMIs) and expressed between 1000 and 7,500 unique genes. In addition, cells were excluded if more than 10% of the determined RNA sequences mapped to mitochondrial genes or if they were classified as doublets by scds (14). In total, 7,728 cells from two RP culture samples, 1,875 cells from RPM cultures, 1,562 cells from RPM (T58A) cultures, 3,401 cells from RPM tumors and 3,463 cells from RPM(T58A) tumors passed these filters for quality. Samples were integrated using Harmony with the top 15 principal components and was run with up to 50 iterations of the algorithm (15). Dimensionality reduction was achieved by creating a Uniform Manifold Approximation and Projection (UMAP) of the first 15 dimensions of harmony integration. Clustering resolution was set at 0.1 for the integrated dataset, resulting in three clusters. Subclustering was conducted in a similar manner and involved re-integration of cells from the neuroendocrine cluster and used identical parameters. Cell type annotation was called using the Azimuth functionality within the Seurat package followed by manual inspection, and enrichment analysis was conducted using enrichR (16). A lung atlas containing 584,884 cells was obtained for Azimuth mediated reference mapping from the HubMap portal (14, 17-24).

Bulk RNA sequencing of the xenograft tumors

Total RNA from the primary and metastatic tumors was isolated using Direct-zol RNA Miniprep kit (Zymo Research). Following RNA isolation, total RNA integrity was checked using a 2100 Bioanalyzer (Agilent Technologies). RNA concentrations were measured using the NanoDrop system (Thermo Fisher Scientific). Preparation of RNA sample library and RNA-seq were performed by the Genomics Core Laboratory at Weill Cornell Medicine or Northwestern University. Messenger RNA was prepared using TruSeq Stranded mRNA Sample Library Preparation kit (Illumina), according to the manufacturer's instructions. The normalized libraries were pooled and sequenced on Illumina Novaseq 6000 sequencer with pair-end 50 cycles. Sequencing adapters were trimmed, and quality metrics were generated using fastp (25). Transcript abundance was quantified by mapping sequencing reads to a reference transcriptome (GENCODE v42, hg38) using Salmon (26).

Differential gene expression and enrichment analysis

Identification of differentially expressed genes involved adjusting for sample identity and *cMYC* expression status when appropriate, and was achieved using model-based analysis of single cell transcriptomics (MAST) (27). Gene set enrichment analysis was conducted by mapping differential expression results to hallmark pathways using clusterProfiler (version 4.0) (28, 29). Cell-level enrichment scores for top 20 cluster markers were previously identified (30) using the AddModuleScore functionality of Seurat. Patterns of *MYC* and *NEUROD1* co-expression were limited to cells in which at least one *MYC* and one *NEUROD1* transcript were detected post-processing.

Deconvolution of bulk RNA sequencing xenografts into SCLC subtypes

Processed single cell RNA-seq data of primary SCLC were obtained from the cellxgene portal (30). Bulk RNA sequencing data for human SCLC tumors (Reads Per Kilobase per Million mapped reads; RPKM) were obtained from cBioPortal. Subtype annotations for 45 patients were obtained from previously published classifications (31). Deconvolution of bulk RNA sequencing data was achieved through BayesPrism (version 2.0) (32). Briefly, single cell transcriptomes from SCLC-A, SCLC-N, SCLC-P and lung adenocarcinoma (LUAD; "NSCLC") samples were annotated as tumor cells. For deconvolution, aggregated tumor annotations were provided as cell type labels and specific tumor types (e.g. SCLC-A) were provided as tumor *states*. BayesPrism received inputs from single cell annotations and associated count matrix, xenograft and primary tumor bulk RNA-sequencing data and was run with outlier.cut=0.01 and outlier.fraction=0.1. Analysis of resultant cell type fractions was limited to SCLC-A, SCLC-N and SCLC-P. Estimated cell type fractions were converted to proportion metrics within the three SCLC subtypes and visualized for concordance with published annotations.

Statistical analyses

Group sample sizes for all in vivo experiments were estimated based off of our previous studies, with at least 5 animals per experimental arm being included for purposes of statistical testing (3-5, 33, 34). For mouse experiments, animals were randomly assigned to each group and no animals were excluded from the analyses. All statistical tests are 2-sided. No adjustments were made for multiple comparisons. The relevant investigators (HJC, EEG and KZ) were blinded to experimental allocations among different experimental arms. For all parametric statistical analyses, data were determined to be normally distributed by the D'Agostino-Pearson test. For comparison between experimental and control groups at a specific time point or tissue site in **Figures 2**, **4**, 5, and

S1, 2-sided Student t-tests, one-way or two-way ANOVA test, Fisher's exact tests and two-sided Kolmogorov–Smirnov test were used in GraphPad Prism. Calculated p-values at or below 2.2×10^{-16} were reported as "$p < 2.2\times10^{-16}$", in line with statistical reporting in R.

Results

Generation of hESC-derived PNEC-like cells that express transgenes encoding CMYC

We used lentivirus vectors encoding doxycycline (DOX)-inducible mRNAs for wildtype (WT) and mutant (T58A) human cMYC (*see Methods*) to infect previously described hESCs from the RUES2 cell line carrying transgenes encoding DOX-inducible short hairpin RNAs (shRNAs) complementary to *TP53* and *RB1*. For simplicity of presentation, we refer to the latter RUES2 cells as RP cells, and the RP cells containing DOX-inducible WT or T58A mutant cMYC as RPM and RPM(T58A) cells throughout the text and figures of this paper.

After growth of infected cells and differentiation into lung cell progenitors (LPs and LCs; **Figure 1A**), we induced pulmonary neuroendocrine cells (PNECs) by inhibition of NOTCH signaling with DAPT, as previously reported (5). The ability of the RPM and RPM(T58A) cells to produce MYC protein was documented by Western Blotting of cell extracts prepared 72 hours after addition of DOX (**Figure 1B**). As expected, both cell lines also contained dramatically reduced amounts of TP53 and RB1 proteins as a result of DOX-induction of shRNAs specific for these tumor suppressor mRNAs (**Figure 1B**).

RUES2-derived PNECs that express WT or T58A cMYC show enhanced oncogenicity as xenografts in the renal capsule of immunodeficient mice

To determine whether production of WT or mutant MYC proteins renders PNECs derived from RPM lines more oncogenic, we sorted CGRP-positive RPM and RPM (T58A) cells from cultures of LCs treated with DAPT and injected the cells subcutaneously or into the renal capsule of immunodeficient mice (the NOG strain: NOD/Shi-scid/IL-2Rγnull) as depicted in **Figure 1A**. The mice were then maintained on diets with or without DOX (*see Methods*). Three to four months later, subcutaneous growths larger than $1000mm^3$ or renal engraftments greater than $100mm^3$ and grossly metastatic lesions in the liver and lungs were tabulated, as summarized in **Figures 1C** and **1D**. As previously reported, PNECs from cultures of RP lines of RUES2 cells produced small benign lesions subcutaneously without invasion or metastasis. Similar findings were observed when these cells were injected into the renal capsule (**Figure 1D**).

Growth of RUES2-derived RPM tumors are DOX-dependent

Thus far, our data suggest that at least some RUES2-derived, PNEC-like cells in which expression of two tumor suppressor genes, *RB1* and *TP53*, is restricted, RP cells, can be transformed into aggressive, metastatic cells by the addition of transgenes encoding WT or mutant cMYC protein (hereafter referred to as "RPM" or "RPM (T58A)" cells). However, we had not directly compared the relative growth rates of these engineered cell types.

We therefore engrafted immunocompromised mice subcutaneously with equivalent numbers of RP, RPM, or RPM (T58A) cells and monitored tumor growth rates. We noted that the volumes of RPM and RPM (T58A)-derived tumors quickly exceeded the volumes of RP-derived tumors (**Figure 2A**). The rapid growth of RPM tumors was dependent on continuous provision of DOX in the diet. If animals on a DOX-free diet were engrafted subcutaneously with RPM or RPM (T58A) cells,

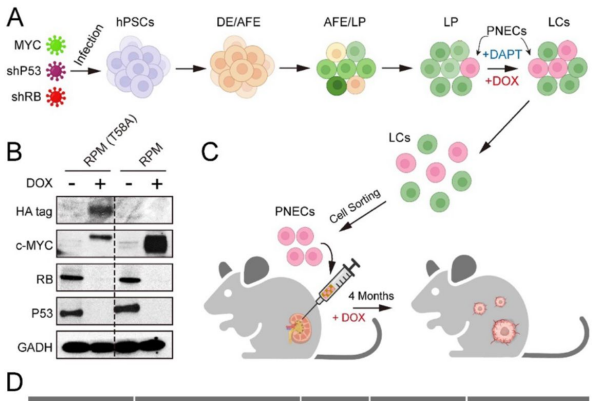

D

Injection site	Genotype of PNECs	Treatment	Primary Tumor# / Injection #	Metastasis
Subcutaneous	RP	**+DOX**	7/12**	None
	RP	-DOX	0/12	None
	RPM	**+DOX**	11/12**	None
	RPM	-DOX	1/12	None
	RPM (T58A)	**+DOX**	10/12**	None
	RPM (T58A)	-DOX	1/12	None
Renal Capsular	RP	**+DOX**	3/6*	None
	RP	-DOX	1/6	None
	RPM	**+DOX**	12/14**	Liver met in 6 mice; Lung met in 1 mice
	RPM	-DOX	2/14	None
	RPM (T58A)	**+DOX**	9/11**	Liver met in 4 mice
	RPM (T58A)	-DOX	2/11	None

Figure 1.

Generation and characterization of hESC-derived lung cells and formation of xenografts with RPM cells.

A) Schematic of the protocol used to generate PNECs by stepwise differentiation of hPSCs to form: definitive endoderm (DE), day 3; anterior foregut endoderm (AFE), day 6; and lung progenitor cells (LPs) days 15 - 25. LPs were further differentiated into the types of lung cells (LCs) found in mature human lung parenchyma and airway epithelium, days 25 - 55. DAPT (10 μM) encourages the formation of PNECs, and addition of doxycycline (1 μM; DOX) induces expression of shRNAs against *RB1* and *TP53* mRNAs, as well as expression of cMYC or cMYC (T58A), as described in the text. **B)** Western blot of extracts of RUES2 LCs at day 25 of differentiation protocol treated with DOX (1 μM for 72hrs); cells unexposed to DOX served as negative expression controls. Apparent differences in cMYC protein levels may be attributable to the HA-tagged version of cMYC (T58A), which migrates slightly slower that wildtype cMYC protein. **C)** Schematic representation of tumorigenesis experiments comparing injection sites (renal capsule or subcutaneous), DOX treatment (+/-DOX diet), and genotypes (see *Methods* for additional details). Total numbers of animals are 6-7 per experimental arm with 2 injection sites per mouse (right and left flank). Renal capsule injections were performed on a single kidney. Transgenic lines of RUES2 hESCs were differentiated and grown in DAPT (10 μM) from days 25 - 55. At day 55, PNECs were separated from other LCs by sorting for PE+ CGRP-expressing cells (*see Methods*). PNECs were then injected either subcutaneously or into the renal capsular space in NOG mice, half of which then received DOX in their feed as described in Materials and Methods. **D)** Table summary of experiments with xenografted mice, indicating the number of animals that developed visible tumors (≥250 mm^3 in volume) at the site of injection or the number of visible metastases in the liver or lung. *, $P < 0.05$; **, $P < 0.01$ by Fisher's test to denote significant differences between mice that did and did not receive DOX diet. As before, abbreviations for cell lines are: RP = shRB1 + shTP53; RPM = shRB1 + shTP53 + WT cMYC; RPM (T58A) = shRB1 + shTP53 + cMYC (T58A).

they failed to produce tumors (**Figure 2B**; *left*). However, tumor growth was observed in some mice engrafted with such cells if the animals were placed on a DOX-containing diet up to one month after injection (**Figure 2B**; *right*). These findings suggest that at least some of the RPM cells remained viable and responsive to the oncogenic effects of depleting RB1 and TP53 and producing cMYC.

The rapid growth and features of RPM and RPM (T58A) tumors in these experiments were histologically consistent with SCLC. Critically, subcutaneous injection did not produce metastastic disease to the liver (*not shown*) nor was there evidence of gross metastases to the lungs in any of the mice examined. (**Figure 2C**). These findings suggest that SCLC-like tumors composed of RUES2-derived RPM cells grow rapidly after subcutaneous implantation, but may require a different microenvironment, such as the vascular rich, highly perfused renal capsule (35, 36), providing a more hospitable environment for metastatic seeding.

Inoculation of the renal capsule facilitates metastasis of the RUES2-derived RPM tumors

RPM tumors, as compared to RP tumors, were notable for increased vascularization, larger volume and invasion into surrounding endothelium (**Figures 3A** to **C**). RPM and RPM (T58A) PNECs injected into the renal capsule of immunocompromised mice also displayed frequent metastasis to the liver (**Figure 3D**). In animals administered DOX, histological examinations showed that approximately half developed metastases in distant organs, including the liver or lung. One of the mice developed metastatic tumors in both liver and lung sites. (**Figure 1D**). No metastases were observed in the bone, brain, or lymph nodes. Metastatic lesions were characterized as having similar proliferative character and expression of cMYC, as well as comparable expression of the neuronal markers NCAM (CD56) and NEUROD1 compared to their paired primary counterparts (**Figures 3E** and **3F**). In contrast, ASCL1 expression was absent in RPM and RPM (T58A) tumors at both primary and metastatic sites (**Figure 3F**). Meanwhile, the majority of cells in RP tumors showed positive ASCL1 expression but lacked NEUROD1 expression (**Figure 3G**). These findings suggest that MYC expression may facilitate the transition of SCLC tumors from the classical ASCL1-driven subtype to the NEUROD1 variant. Thus, both the site of implantation of cells and the addition of a driver oncogene were required to produce vigorous growth and metastatic spread of SCLC-like tumors, and the metastatic lesions retained histological and immunohistochemical features of the primary tumors.

RUES2-derived RPM tumors most closely resemble the NEUROD1-high (SCLC-N) subtype of SCLC

To better understand the characteristics of RUES2-derived RPM tumors, we performed single-cell RNA-sequencing on culture-derived (“2D”) and tumor-derived RPM and RPM (T58A) viable EGFP+ cells. By integrating previously published RUES2-derived RP single cell data (5), we observed three dominant cell-type groups in transcriptional space, using reference-mapping, enrichment analysis and manual curation to identify cell lineage likelihood: a basal-like cluster marked by expression of *KRT19*, a fibroblast-like cluster marked by expression of *COL1A1*, and the most prominent cluster of cells appearing to have features of neuroendocrine differentiation, marked by expression of the neuroendocrine lineage defining transcription factor *ASCL1* (**Figure 4A** and **Supplemental Table 1**). Comparing the recently described SCLC subtype markers (31) across these datasets showed that cells within the neuroendocrine differentiation cluster cells expressed *ASCL1* and *NEUROD1*, whereas *POU2F3* RNA was not detected. Levels of *YAP1* RNA were variable and were not co-expressed with either *ASCL1* or *NEUROD1* (**Figure 4B**). *YAP1* expression was mostly attributed to fibroblast- and basal-like cells that are often observed in long-term cultures of differentiated hESCs (**Figure 4B**) (4, 37-39).

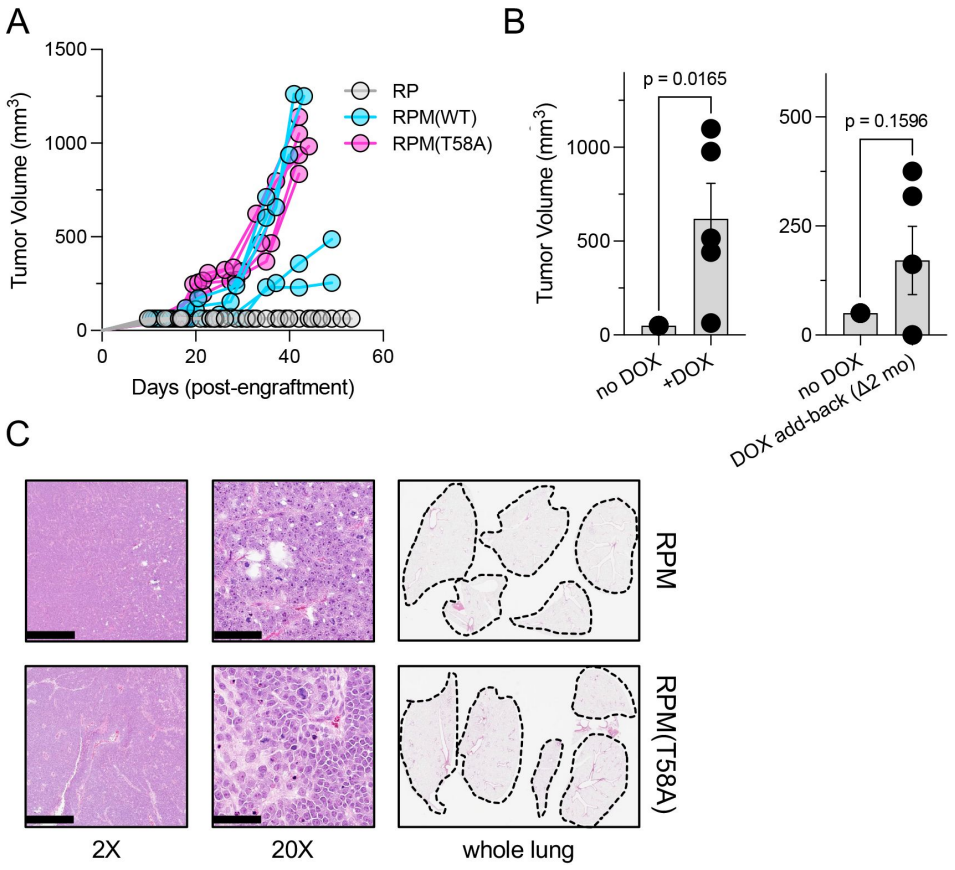

Figure 2.

Dox-dependent growth of RUES2-derived RPM and RPM (T58A) subcutaneous tumors.

A) Subcutaneous engraftment of 10^6 viable cells at ~ day 50 of RUES2 lung differentiation protocol from indicated genotypes. Cells were cultured in the presence of media containing 1 μM DOX and 10 μM DAPT from days 25 – 55. All immunocompromised mice were maintained on DOX diet throughout this study; n=5/arm. **B)** *Left*: subcutaneous engraftment of 10^6 viable RPM tumor cells from the first passage (mouse-to-mouse passage) into immunocompromised mice (NSG) maintained on DOX or normal chow; n=5 animals per arm with single flank engraftments, +/-standard error of the mean (SEM). $^{**}P < 0.05$. *Right:* after one month on normal chow, mice were placed on DOX chow (DOX "add-back"); tumor volumes were measured one month later (2 months on study). Paired t test p values are shown for each comparison. **C)** Representative H&E tumor histology from RPM or RPM (T58A) engraftments; 2X (scalebar 1mm) and 20X (scalebar 100um). Representative whole lung sagittal sections showed no evidence of gross metastasis from flank injections at study endpoints; n=3 analyzed per genotype. Dashed lines shown for boundaries of lung lobes.

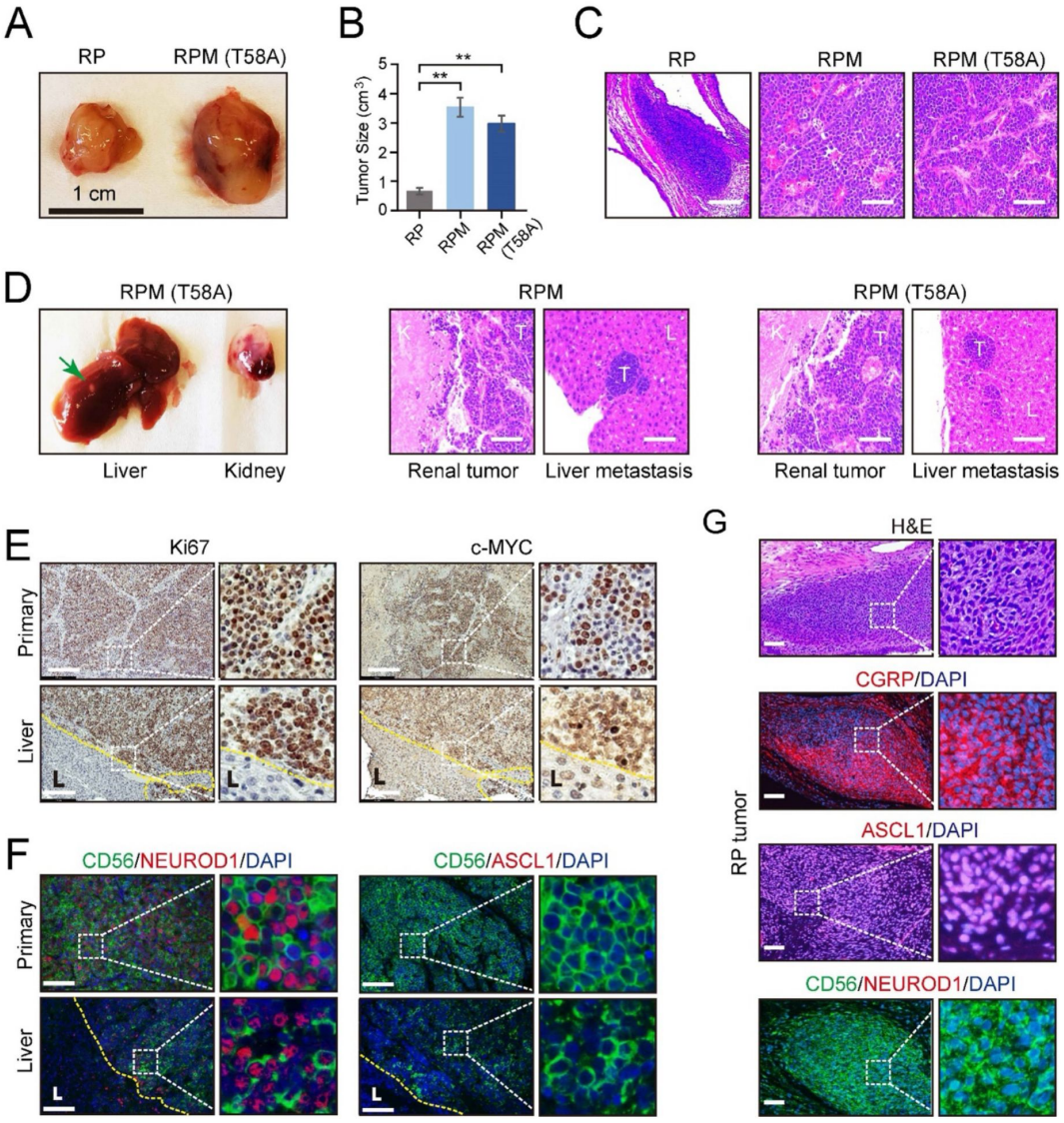

Figure 3.

Effects of cMYC on the gross and histopathological appearance of xenografts grown in immunodeficient mice fed with DOX for 3-4 months.

A) Subcutaneous xenografts formed with hESC-derived PNECs with RP, RPM or RPM (T58A) genotypes. Photographs of representative tumors formed with cells of the indicated genotypes are shown for RP and RPM; indicated scale of 1cm. **B)** Quantification of the tumor sizes and paired comparisons for a secondary *in vivo* experiment; n=5 animals per arm with single subcutaneous engraftmetns; **P<0.01. **C)** H&E staining of the indicated tumors from panel *B*. **D)** Gross and histologic pathology of renal capsular xenografts and liver metastases formed with the RPM or RPM (T58A) cells. Left panels, gross appearance of representative tumors within the liver (metastasis) or kidney (primary); right panels, H&E staining of primary and metastatic tumors (T) formed in kidney (K) and liver (L) in the RPM (left) or RPM (T58A) model. **E)** Immunostaining of tumor samples from *D*. Samples of primary peri-renal tumors and hepatic metastases in mice injected with hESC-derived PNECs programmed to reduce levels of *TP53* and *RB1* mRNA and to express wild type MYC were stained with antisera for Ki67 (*left*) or MYC (*right*). **F)** Immunofluorescence staining for neuroendocrine markers ASCL1, NEUROD1 and CD56 from sections in *E* of the RPM tumors. **G)** Immunofluorescence staining for neuroendocrine markers, CGRP, ASCL1, NEUROD1 and CD56 in the RP tumors. H&E staining serves as the bright-field comparison of the indicated tumors.

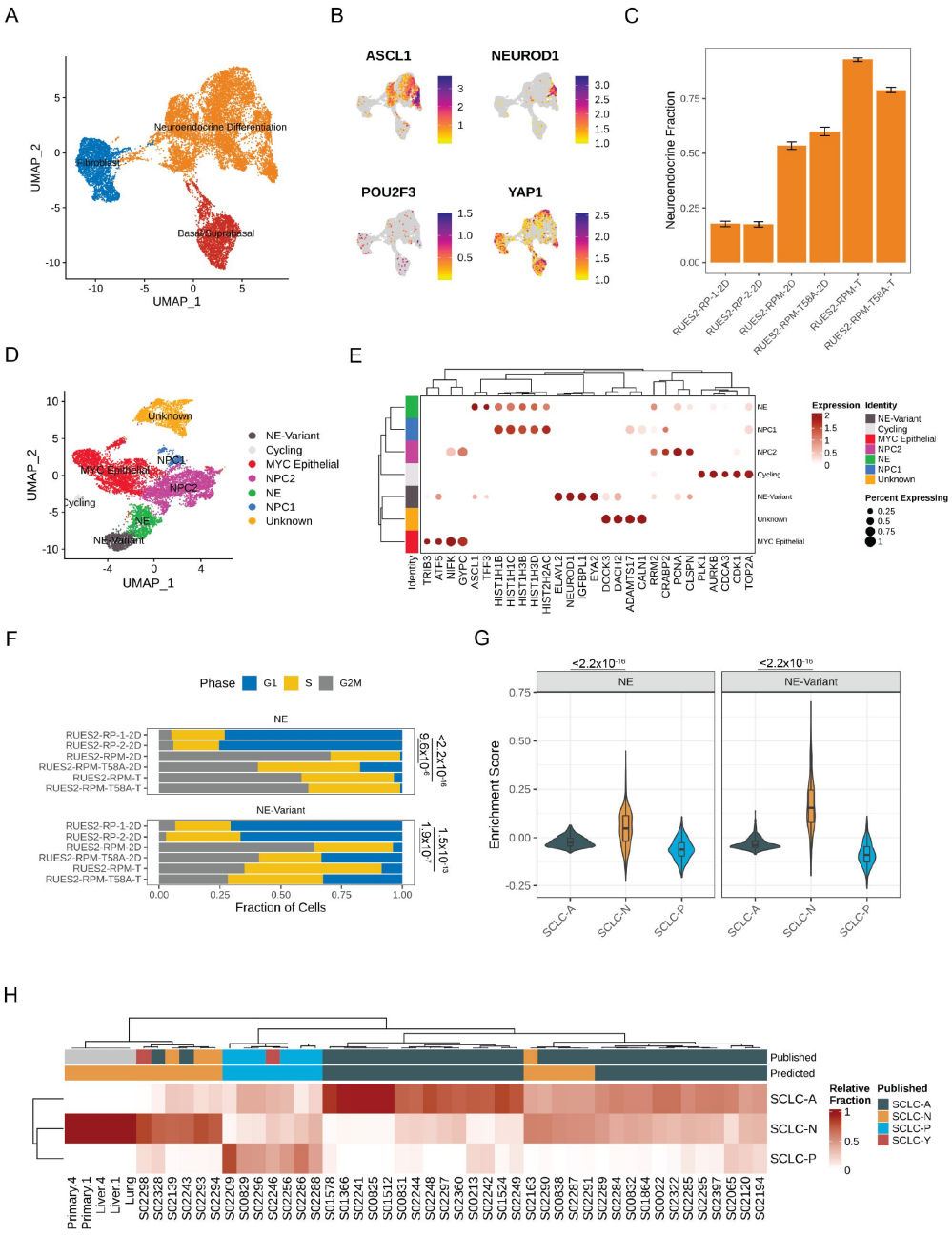

Figure 4.

Single cell and bulk RNA profiling of RUES2-derived RPM tumors and comparison with primary human SCLC.

A) UMAP projection of cultured RP samples from Chen et al (2019) and RPM samples [*this study*] with 3 major cellular lineages annotated by color. **B)** Expression of SCLC subtype markers across dataset in *A*. **C)** Neuroendocrine fraction of cells by sample ID. **D)** Subclustering of the "neuroendocrine differentiation" cluster from *A*. **E)** Dot plot of differential cluster markers in the subclustering analysis from *E*. **F)** Cell cycle evaluation of NE and NE-Variant clusters indicated by color and fraction of cells. **G)** SCLC subtype enrichment scores from Chan et al (2021); cluster markers in NE and NE-Variant cells from RPM tumors. **H)** Bulk RNA-sequencing subtype estimation based on Chan et al (2021) SCLC subtypes from RPM primary or metstatic tumors as compared to published primary SCLC data. Published labels were obtained from Rudin et al (2019). Bulk patient RNA-sequencing data (reads per kilobase per million mapped reads (RPKM)) were compared to bulk RNA-sequencing of select RPM tumors and metastatic samples. Primary tumor and liver metastases were obtained from two pairs (animals #1 and #4) of mice engrafted with RUES2-derived RPM tumor cells into the renal capsule and grossly macro-dissected during necropsy.

Next, we asked whether the over-expression of *MYC* in RPM cells was associated with increased neuroendocrine differentiation when compared to cell lines that did not contain c*MYC* transgenes (i.e. RP cells). One notable difference between our prior work and this study was our attempt to increase the tumor cell component of the RPM and RPM (T58A) samples by sorting cells for high EGFP expression. EGFP is expressed in *cis* with the *RB1* targeting shRNA; however, EGFP is not expressed uniformly across all cells following the differentiation protocol, suggesting some cells may silence the integrated vector. We performed differential cluster abundance analysis after accounting for the fraction of cells that were EGFP+ during cell sorting. These results indicated that RPM cell lines (WT or T58A) were associated with a two-fold increase in the neuroendocrine compartment when compared with RP cells ($p < 2.2\times10^{-16}$; **Figure 4C** and **Supplemental Figures 1A** and **1B**). Similarly, RPM tumors had a three-fold enrichment of cells expressing neuroendocrine markers compared to RP cell lines ($p < 2.2\times10^{-16}$). Notably, we found that RPM tumors and cells expressed *MYC*, not *MYCN* or *MYCL* at high levels (**Supplemental Figure 1C**). Moreover, *EGFP* expression was strongly correlated with *MYC* (Pearson r = 0.45, p < 2.2×10-16) and not *MYCN* (Pearson r = 0.00043, p = 0.97) nor *MYCL* (Pearson r = −0.031, p = 0.002). Together, these results suggest that the over-expression of either WT or T58A MYC yielded a larger neuroendocrine compartment.

By sub-clustering the neuroendocrine differentiation group, we could clearly identify *ASCL1*-high and *NEUROD1*-high compartments, as well as several other groups of cycling cells that did not cleanly fit into any lung lineage cell identity (**Figure 4D**, **Supplemental Table 2**). We conducted differential gene expression to further characterize the *NEUROD1*-high (abbreviated “NE-variant”) and *ASCL1*-high (abbreivated “NE”) clusters observed with RPM cells (from cell lines and tumors) and found that the NE-variant cluster was associated with increased expression of genes highly expressed in variant small cell lung cancer (*NEUROD1, SCG3, IGFBPL1, SSTR2* and c*MYC)* (**Supplemental Figure 1D**, **Supplemental Table 3**). In contrast, the NE (or “NE-classic”) cluster was linked to heightened expression of a variety of genes ranging from histones (*HISTH1B, HISTH1D*) to redox processes (*MT1E, MT2A*) (**Figure 4E**). Gene set enrichment analysis of these results in the NE-variant cluster revealed increased expression of genes associated with activation of epithelial-mesenchymal transition (EMT; $p = 6.81\times10^{-3}$) and pancreatic beta cell signaling ($p = 1.01\times10^{-3}$). However, this cluster was also linked to lower levels of oxidative phosphorylation ($p = 1.07\times10^{-25}$), possibly suggesting these sub-groups of cells are biologically different (**Supplemental Figure 1E**). Further examination of the *ASCL1*-high and *NEUROD1*-high clusters revealed that, across both clusters, RPM and RPM (T58A) cells were associated with higher expression of genes associated with cells in dividing phases of the cell cycle than were observed RP cultures. We compared the proportion of G2M cells between culture-derived RPM and RP models. This revealed that RPM cells were associated with a 10- and 11-fold increase in the NE and NE-variant clusters respectively (NE $p = 9.6\times10^{-6}$, NE-Variant $p = 1.9\times10^{-7}$) with a relative reduction in cells in the G1 phase (**Figure 4F**). Similar trends were observed from data in human tumors (NE $p < 2.2\times10^{-16}$, NE-Variant $p = 1.5\times10^{-13}$, **Figure 4F**).

Given the striking increase in proliferation in cMYC producing cells, we sought to understand the association between c*MYC* and *ASCL1* or *NEUROD1* expression. We computed the cellular density of co-expression patterns of cells that express c*MYC* in addition to either *ASCL1* or *NEUROD1*. This identified that the joint density was highest for cells that co-express c*MYC* and *NEUROD1* and was localized to the *NEUROD1*-high cluster (**Supplemental Figure 1F**). In comparison, c*MYC* and *ASCL1* co-expression patterns were heterogenous, and found in the *ASCL1*-high cluster as well as in cells that could not be annotated with confidence. Similar to previously reported by other groups, we found that *ASCL1* and *MYC* expression are negatively correlated (Pearson r = −0.11, $p = 1.5\times10^{-4}$). Moreover, modest correlation between c*MYC* and *NEUROD1* expression was identified in our single cell data (Pearson r = 0.17, $p = 3.7\times10^{-4}$, **Supplemental Figure 1G**). Given that single cell sequencing experiments suffer from a high dropout rate, we attempted to validate c*MYC* and *NEUROD1* co-expression patterns in bulk primary and metastatic RPM tumors. Although we couldn’t determine co-expression within the same cell using bulk gene expression data, we

identified an extremely strong correlation between the expression of these two genes (Pearson r = 0.93, p = 0.02, **Supplemental Figure 1H**). Taken together, we show that the over-expression of *MYC* (WT or T58A) may be linked to an SCLC-N phenotype.

Upon identification of the *ASCL1*- and *NEUROD1*-high clusters, we sought to further characterize how closely they resemble SCLC tumors transcriptionally using a two-pronged approach. First, we overlayed SCLC-A, SCLC-N and SCLC-P signatures (30) from our single cell data and calculated subtype enrichment scores. Enrichment patterns in RPM and RPM (T58A) xenografts revealed that both *ASCL1*- and *NEUROD1*-high clusters expressed SCLC-N-associated genes more frequently than SCLC-A and SCLC-P-associated counterparts ($p < 2.2\times10^{-16}$, **Figure 4G**). In contrast, RP cell cultures more closely resembled cells from tumors with an SCLC-A phenotype ($p < 2.2\times10^{-16}$, **Supplemental Figure 1I**). Second, we identified the transcriptional identity of RPM xenografts and paired metastases by cellular deconvolution. Bulk gene expression of RPM tumors along with human SCLC biopsies (40) were deconvolved into SCLC subtypes. This identified relative cellular proportions of SCLC subtypes in bulk RNA-seq data. Overall, we found high concordance with published subtype annotations and those predicted by our analysis (**Figure 4H**) (31). Moreover, we found that all RPM xenografts strongly exhibited an SCLC-N transcriptional program. Taken together, these data suggest that over-expression of wild type or mutant *MYC* alters the transcriptional identity of RP cells, encouraging neuroendocrine differentiation, and may assist with the transformation from a SCLC-A to SCLC-N phenotype.

Discussion

In this report, we show that the addition of an efficiently expressed transgene encoding normal or mutant human cMYC can convert weakly tumorigenic human PNEC cells, derived from a human ESC line and depleted of tumor suppressors RB1 and TP53, into highly malignant, metastatic SCLC-like cancers after implantation into the renal capsule of immunodeficient mice.

Experimental models for understanding the origins, behaviors, and control of human cancers have been developed in numerous ways for more than a century. Some of the models depend on producing tumors in animals or transforming the behavior of cells growing in culture with viruses, chemical agents, genetic changes, or other perturbations, or by deriving cells from human cancers and growing them in animals or in tissue culture. The choice of these approaches have been influenced by the goals of the research, the type of cancer under study, and available technologies.

Because SCLC is a highly aggressive cancer with a relatively stereotypic genotype that is generally recalcitrant to therapeutic strategies that have not changed appreciably in the past thirty years, we have been attempting to generate a model for SCLC in which the cancer cells are human in origin, derived from the most commonly affected pulmonary cell lineage (neuroendocrine), and equipped with the major and most common genotypic and phenotypic changes characteristic of SCLC.

The most obvious use of these cells (the RPM lines described here) is for the evaluation of the efficacy of novel therapeutic agents acting directly on tumor cells during growth in culture or during growth as xenografts in immunosuppressed mice. However, our attempts to conduct therapeutic studies with the RPM lines have not been sufficiently extensive or rigorous to warrant presentation here. In addition, treatment strategies that involve host elements other than the tumor itself, such as immune cells or other features of the tumor micro-environment, might require an experimental platform more complex that those that we have constructed.

Our choice of cMYC to serve as an oncogenic driver in hESC-derived PNECs was based on both the frequent finding of high levels of *cMYC* RNA in human SCLC and the use of Myc over-expression strategies to generate aggressive mouse models of SCLC (7, 8, 41-43). However, not all human SCLC

tumors have abundant *cMYC* RNA, and other genes, including other members of the MYC gene family, have been implicated in the pathogenesis of SCLC. So it will be interesting to compare the ability of transgenes encoding other MYC proteins, such as *NMYC* and *LMYC*, as well as other oncoproteins (both those implicated and not implicated in human SCLC carcinogenesis) to convert RP cells into malignant tumors and to produce metastatic phenotypes, as we have observed here with RPM cells. In particular, it may be important to determine whether hESC-derived SCLC cells with varied genotypes are liable to metastasize to specific sites such as the brain and bone, which are commonly affected in patients with SCLC, but were not sites for metatastic growth in the experiments reported here. Finally, the role of other tumor suppressor genes, such as *PTEN* – implicated in the development of mouse models of histological transformation of LUAD to SCLC that we have recently reported (44) – should also be examined in this human ESC-derived model.

We have used transcriptional profiling as a means to compare human ESC-derived SCLC grown from RPM cells with SCLC tumor samples from patients. Other aspects of tumor cell behavior – including pathophysiological features, responses to therapeutic strategies, and the appearance of molecular, metabolic, and immunological markers – might also provide means to determine the degree of similarity between this novel stem cell-derived model and genuine human neoplasms.

Transcriptional profiling has also allowed us to conclude that the hESC-derived tumors arising from RPM RUES2 cells belong to the SCLC-N subtype, one of the major subtypes of SCLC now recognized by several laboratories and clinicians studying SCLC. It is unclear whether SCLC-N truly represents a subtype of SCLC with distinct outcomes and therapeutic sensitivities (45), or rather a snapshop from a continuum in tumor evolution driven [principally] by *MYC* towards an aggressive, recalcitrant disease (46, 47). Future studies of stem cell-derived SCLC should consider ways to generate tumors that model the other common subtypes including SCLC-P and SCLC-I ("inflamed" SCLC) (45). This might be achieved by altering the cancer genotype, by using a differentiation scheme that produces physiologically varied precursor cells, or by employing a wider variety of hESCs to develop SCLCs.

Finally, we note that in the experiments reported here metastatic spread was observed from RPM tumors growing initially in the renal capsule but not from primary subcutaneous tumors initiated with the same cell culture. It may prove important to test other sites of primary tumor growth with RPM cells from the RUES2 line or with other SCLC models, to determine the degree to which metastatic spread depends on the site(s) of growth of the primary tumor and to identify specific factors that promote such spread.

Author Contributions

H.J.C., E.E.G., K.Z. and A.T. performed wet lab experiments. Y.S. and O.E. performed computational analyses, including single cell RNA-sequencing data analysis. All authors participated in the design and interpretation of some or all experiments. H.V., H.J.C., and E.E.G. wrote the manuscript, and all authors suggested editorial changes. H.V. and H.J.C. conceived the study and recruited the collaborating partners.

Acknowledgements

We thank Oksana Mashadova and Sukanya Goswami in the Varmus Laboratory for technical support, Arun Unni and John Ferrarone in the Varmus Laboratory and Jonathan Chen in the Chen Laboratory for useful advice. Supported by awards to H.V. and O.E. from the US Department of Defense (LC160136) and the U.S. National Cancer Institute (U01CA224326), funds from the Meyer

Cancer Center, Weill Cornell Medicine (to H.V.), and a K99/R00 NIH Pathway to Independence Award (4R00CA226353), US Department of Defense (RA220012) and a Lung Cancer Research Foundation (LCRF) Pilot Project Award (to H.J.C.).

Competing Financial Interests

O.E. is scientific adviser for, and an equity holder in, Freenome, Owkin, Volastra Therapeutics, OneThree Biotech, Genetic Intelligence, Acuamark DX, Harmonic Discovery, and Champions Oncology, and has received funding from Eli Lilly, Johnson and Johnson - Janssen, Sanofi, AstraZeneca, and Volastra. H.V. is a member of the SABs of Dragonfly Therapeutics and Surrozen. None of these companies are currently providing support for the Varmus laboratory. All other authors declare no competing interests.

Supplemental figures

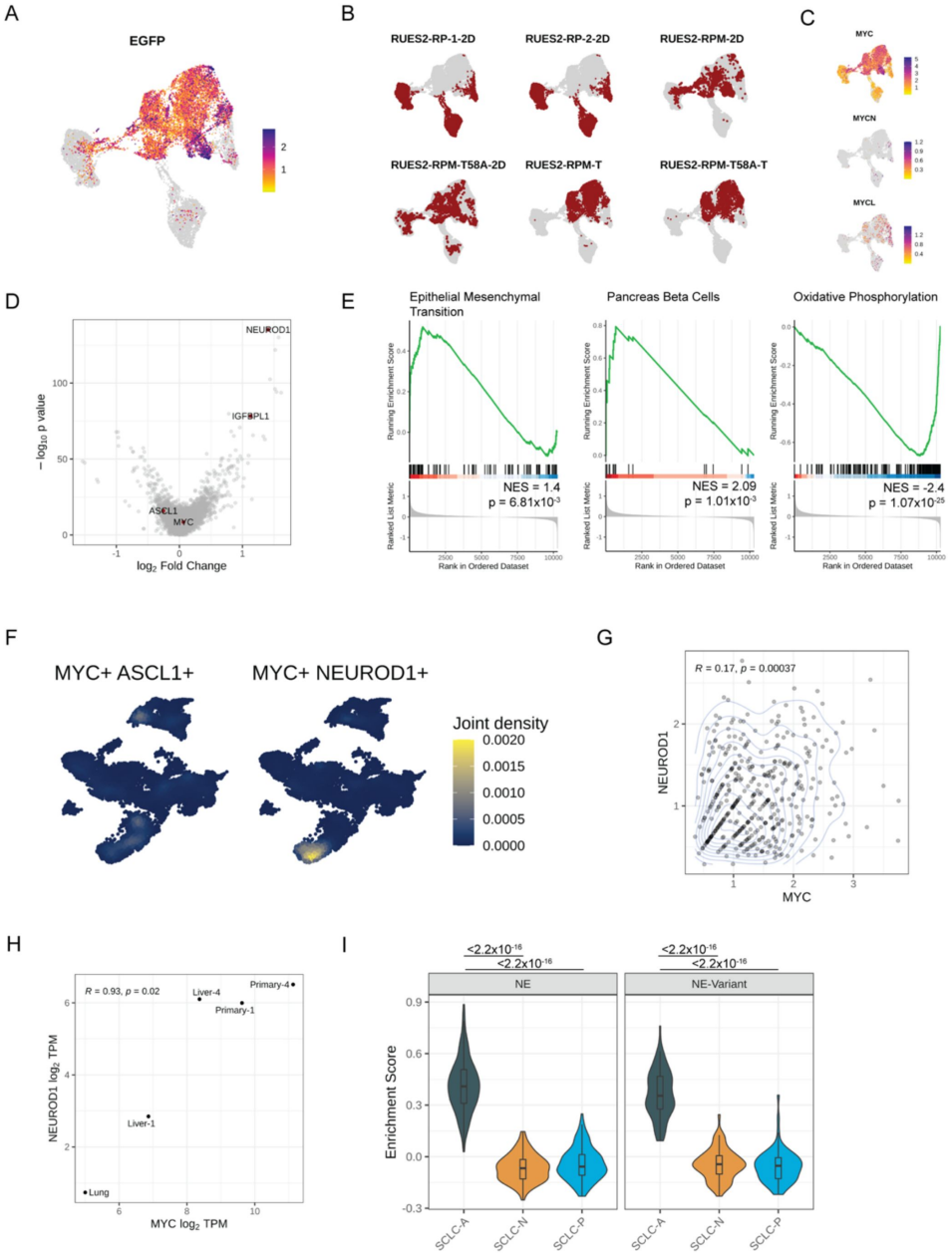

Supplemental Figure 1.

Gene expression and characterization of RUES2-derived tumors.

A) *EGFP* expression across the full dataset integrating RP and RPM cells in addition to RPM tumor cells. **B**) Individual sample IDs and relative contribution (weighted; red) to initial clustering distribution for the 6 sample sets used in this combined analysis. **C)** *MYC, MYCN* and *MYCL* expression across the full dataset **D)** Differential gene expression (DEG) between NE-Variant and NE cluster. Select genes are called out in red. **E)** Select gene set enrichment analysis for top 3 differentially expressed programs between *NEUROD1*-high (NE-variant) and *ASCL1*-high (NE) subsets of cells from only RPM tumor cells; shown as normalized enrichment scores (NES). Positive enrichment is greater activation in the NE-Variant subset (i.e. the *NEUROD1*+ subset), whereas negative enrichment is greater in the NE subset. **F)** Cellular density of co-expression patterns for *ASCL1* and *NEUROD1* across the neuroendocrine differentiation subset. **G)** Scatter density plot of *MYC* and *NEUROD1* expression across all cells in the neuroendocrine differentiation cluster. **H)** Plot of *MYC* and *NEUROD1* expression in bulk expression data derived from RPM tumors; data are shown as log2 of transcripts per million (TPM). **I)** Enrichment score for SCLC subtype markers in NE and NE-Variant cells from RP cell cultures (2D), demonstrating preferably enrichment of the SCLC-A subtype in the absence of over-expression of a *MYC* transgene.

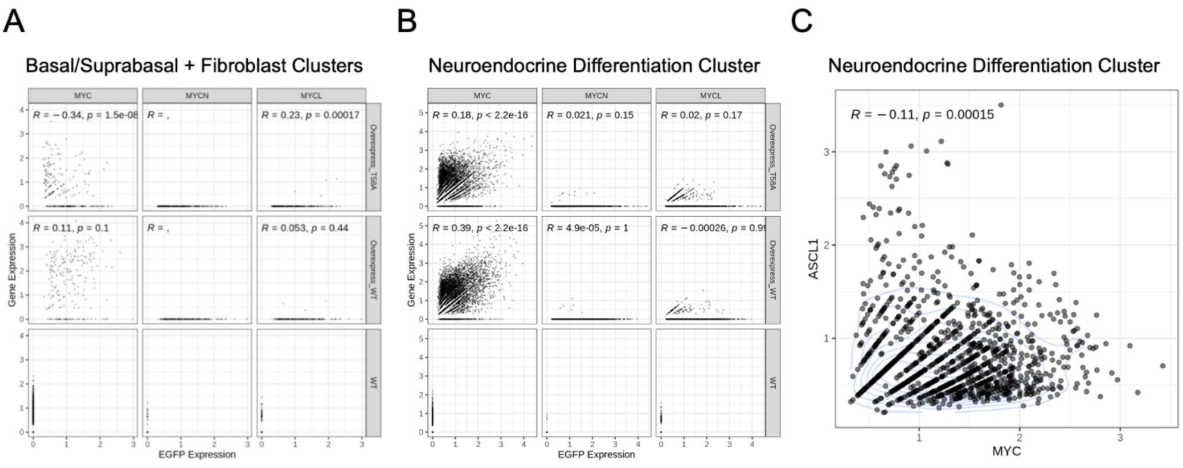

Supplemental Figure 2.

MYC family member expression correlates in RUES2-derived RPM tumors.

A) Expression correlation of *EGFP* for *MYC, MYCN* or *MYCL1* from the neuroendocrine differentiation cluster identified in **Figure 4A**. **B)** Similar to A, but now for the neuroendocrine differentiation cluster. Scatter plots depict correlation in NE and non-NE clusters. **C)** Expression correlation of *ASCL1* and *MYC* in the neuroendocrine differentiation cluster. All sample pools were included in this correlation. Each data point is a single cell. Correlation (*R* value) and significance (*P* value) shown for each individual comparison.

References

1. Varmus H., Weinberg R. A. (1993) **Genes and the biology of cancer, Scientific American Library series; no. 42** New York: Scientific American Library : Distributed by W.H. Freeman and Co

2. Funato K., Major T., Lewis P. W., Allis C. D., Tabar V. (2014) **Use of human embryonic stem cells to model pediatric gliomas with H3.3K27M histone mutation** *Science* **346**:1529–1533

3. Huang S. X., et al. (2015) **The in vitro generation of lung and airway progenitor cells from human pluripotent stem cells** *Nat Protoc* **10**:413–425

4. Huang S. X., et al. (2014) **Efficient generation of lung and airway epithelial cells from human pluripotent stem cells** *Nat Biotechnol* **32**:84–91

5. Chen H. J., et al. (2019) **Generation of pulmonary neuroendocrine cells and SCLC-like tumors from human embryonic stem cells** *J Exp Med* **216**:674–687

6. Budczies J., et al. (2015) **The landscape of metastatic progression patterns across major human cancers** *Oncotarget* **6**:570–583

7. Ireland A. S., et al. (2020) **MYC Drives Temporal Evolution of Small Cell Lung Cancer Subtypes by Reprogramming Neuroendocrine Fate** *Cancer Cell* **38**:60–78

8. Mollaoglu G., et al. (2017) **MYC Drives Progression of Small Cell Lung Cancer to a Variant Neuroendocrine Subtype with Vulnerability to Aurora Kinase Inhibition** *Cancer Cell* **31**:270–285

9. Conklin J. F., Baker J., Sage J. (2012) **The RB family is required for the self-renewal and survival of human embryonic stem cells** *Nature communications* **3**

10. Chen H. J., et al. (2015) **Comprehensive models of human primary and metastatic colorectal tumors in immunodeficient and immunocompetent mice by chemokine targeting** *Nature biotechnology* **33**:656–660

11. Chen H. J., et al. (2012) **Chemokine 25-induced signaling suppresses colon cancer invasion and metastasis** *The Journal of clinical investigation* **122**:3184–3196

12. He D., Patro R. (2023) **simpleaf: A simple, flexible, and scalable framework for single-cell transcriptomics data processing using alevin-fry** *bioRxiv* https://doi.org/10.1101/2023.03.28.534653

13. Hao Y., et al. (2021) **Integrated analysis of multimodal single-cell data** *Cell* **184**:3573–3587

14. Bais A. S., Kostka D. (2020) **scds: computational annotation of doublets in single-cell RNA sequencing data** *Bioinformatics* **36**:1150–1158

15. Korsunsky I., et al. (2019) **Fast, sensitive and accurate integration of single-cell data with Harmony** *Nat Methods* **16**:1289–1296

16. Chen E. Y., et al. (2013) **Enrichr: interactive and collaborative HTML5 gene list enrichment analysis tool** *BMC Bioinformatics* **14**

17. Deprez M., et al. (2020) **A Single-Cell Atlas of the Human Healthy Airways** *Am J Respir Crit Care Med* **202**:1636–1645

18. Goldfarbmuren K. C., et al. (2020) **Dissecting the cellular specificity of smoking effects and reconstructing lineages in the human airway epithelium** *Nat Commun* **11**

19. Habermann A. C., et al. (2020) **Single-cell RNA sequencing reveals profibrotic roles of distinct epithelial and mesenchymal lineages in pulmonary fibrosis** *Sci Adv* **6**

20. Madissoon E., et al. (2019) **scRNA-seq assessment of the human lung, spleen, and esophagus tissue stability after cold preservation** *Genome Biol* **21**

21. Morse C., et al. (2019) **Proliferating SPP1/MERTK-expressing macrophages in idiopathic pulmonary fibrosis** *Eur Respir J* **4**

22. Schupp J. C., et al. (2021) **Integrated Single-Cell Atlas of Endothelial Cells of the Human Lung** *Circulation* **144**:286–302

23. Travaglini K. J., et al. (2020) **A molecular cell atlas of the human lung from single-cell RNA sequencing** *Nature* **587**:619–625

24. Braga F. A. Vieira, et al. (2019) **A cellular census of human lungs identifies novel cell states in health and in asthma** *Nat Med* **25**:1153–1163

25. Chen S., Zhou Y., Chen Y., Gu J. (2018) **fastp: an ultra-fast all-in-one FASTQ preprocessor** *Bioinformatics* **34**:i884–i890

26. Patro R., Duggal G., Love M. I., Irizarry R. A., Kingsford C. (2017) **Salmon provides fast and bias-aware quantification of transcript expression** *Nat Methods* **14**:417–419

27. Finak G., et al. (2015) **MAST: a flexible statistical framework for assessing transcriptional changes and characterizing heterogeneity in single-cell RNA sequencing data** *Genome Biol* **16**

28. Liberzon A., et al. (2015) **The Molecular Signatures Database (MSigDB) hallmark gene set collection** *Cell Syst* **1**:417–425

29. Wu T., et al. (2021) **clusterProfiler 4.0: A universal enrichment tool for interpreting omics data** *Innovation (Camb)* **2**

30. Chan J. M., et al. (2021) **Signatures of plasticity, metastasis, and immunosuppression in an atlas of human small cell lung cancer** *Cancer Cell* **39**:1479–1496

31. Rudin C. M., et al. (2019) **Molecular subtypes of small cell lung cancer: a synthesis of human and mouse model data** *Nat Rev Cancer* **19**:289–297

32. Chu T., Wang Z., Pe'er D., Danko C. G. (2022) **Cell type and gene expression deconvolution with BayesPrism enables Bayesian integrative analysis across bulk and single-cell RNA sequencing in oncology** *Nat Cancer* **3**:505–517

33. Chen H. J., et al. (2016) **A recellularized human colon model identifies cancer driver genes** *Nature biotechnology* **34**:845–851

34. Unni A. M., Lockwood W. W., Zejnullahu K., Lee-Lin S. Q., Varmus H. (2015) **Evidence that synthetic lethality underlies the mutual exclusivity of oncogenic KRAS and EGFR mutations in lung adenocarcinoma** *Elife* **4**

35. Bogden A. E., et al. (1979) **Growth of human tumor xenografts implanted under the renal capsule of normal immunocompetent mice** *Exp Cell Biol* **47**:281–293

36. Sobczuk P., et al. (2020) **Choosing The Right Animal Model for Renal Cancer Research** *Transl Oncol* **13**

37. Chen Y. W., et al. (2017) **A three-dimensional model of human lung development and disease from pluripotent stem cells** *Nat Cell Biol* **19**:542–549

38. Dye B. R., et al. (2015) **In vitro generation of human pluripotent stem cell derived lung organoids** *Elife* **4**

39. Toste de Carvalho A. L., et al. (2021) **The in vitro multilineage differentiation and maturation of lung and airway cells from human pluripotent stem cell-derived lung progenitors in 3D** *Nat Protoc* **16**:1802–1829

40. George J., et al. (2015) **Comprehensive genomic profiles of small cell lung cancer** *Nature* **524**:47–53

41. Huijbers I. J., et al. (2014) **Rapid target gene validation in complex cancer mouse models using re-derived embryonic stem cells** *EMBO Mol Med* **6**:212–225

42. Ciampricotti M., et al. (2021) **Rlf-Mycl Gene Fusion Drives Tumorigenesis and Metastasis in a Mouse Model of Small Cell Lung Cancer** *Cancer Discov* **11**:3214–3229

43. Kim D. W., et al. (2016) **Genetic requirement for Mycl and efficacy of RNA Pol I inhibition in mouse models of small cell lung cancer** *Genes Dev* **30**:1289–1299

44. Gardner E. E., et al. (2023) **Lineage-specific intolerance to oncogenic drivers restricts histological transformation** *bioRxiv* https://doi.org/10.1101/2023.06.21.545980

45. Gay C. M., et al. (2021) **Patterns of transcription factor programs and immune pathway activation define four major subtypes of SCLC with distinct therapeutic vulnerabilities** *Cancer Cell* **39**:346–360

46. Choudhuri S. P., et al. (2023) **Acquired Cross-resistance in Small Cell Lung Cancer due to Extrachromosomal DNA Amplification of MYC paralogs** *bioRxiv* https://doi.org/10.1101/2023.06.23.546278

47. Pongor L. S., et al. (2023) **Extrachromosomal DNA Amplification Contributes to Small Cell Lung Cancer Heterogeneity and Is Associated with Worse Outcomes** *Cancer Discov* **13**:928–949

Author information

Huanhuan Joyce Chen*

Meyer Cancer Center, Weill Cornell Medicine, New York, USA., The Pritzker School of Molecular Engineering, The University of Chicago, Chicago, USA., The Ben May Department for Cancer Research, The University of Chicago, Chicago, USA
ORCID iD: 0000-0002-1446-7184

For correspondence: joycechen@uchicago.edu
*contributed equally

Eric E Gardner*

Meyer Cancer Center, Weill Cornell Medicine, New York, USA.
ORCID iD: 0000-0002-1552-2675

*contributed equally

Yajas Shah

Caryl and Israel Englander Institute for Precision Medicine, Weill Cornell Medicine, New York, USA.
ORCID iD: 0000-0002-9692-4878

Kui Zhang

The Pritzker School of Molecular Engineering, The University of Chicago, Chicago, USA., The Ben May Department for Cancer Research, The University of Chicago, Chicago, USA
ORCID iD: 0000-0001-9618-610X

Abhimanyu Thakur

The Pritzker School of Molecular Engineering, The University of Chicago, Chicago, USA., The Ben May Department for Cancer Research, The University of Chicago, Chicago, USA
ORCID iD: 0000-0002-0846-0998

Chen Zhang

Department of Pathology and Laboratory Medicine, Weill Cornell Medicine, New York, USA.

Olivier Elemento

Caryl and Israel Englander Institute for Precision Medicine, Weill Cornell Medicine, New York, USA.
ORCID iD: 0000-0002-8061-9617

Harold Varmus

Meyer Cancer Center, Weill Cornell Medicine, New York, USA.
ORCID iD: 0000-0002-6444-1943

For correspondence: varmus@med.cornell.edu

Editors

Reviewer #1 (Public review):

Summary:

The authors introduced their previous paper with the concise statement that "the relationships between lineage-specific attributes and genotypic differences of tumors are not understood" (Chen et al., JEM 2019, PMID: 30737256). For example, it is not clear why combined loss of RB1 and TP53 is required for tumorigenesis in SCLC or other aggressive neuroendocrine (NE) cancers, or why the oncogenic mutations in KRAS or EGFR that drive NSCLC tumorigenesis are found so infrequently in SCLC. This is the main question addressed by the previous and current papers.

One approach to this question is to identify a discrete set of genetic/biochemical manipulations that are sufficient to transform non-malignant human cells into SCLC-like tumors. One group reported transformation of primary human bronchial epithelial cells into NE tumors through a complex lentiviral cocktail involving inactivation of pRB and p53 and activation of AKT, cMYC and BCL2 (PARCB) (Park et al., Science 2018, PMID: 30287662). The cocktail previously reported by Chen and colleagues to transform human pluripotent stem-cell (hPSC)-derived lung progenitors (LPs) into NE xenografts was more concise: DAPT to inactivate NOTCH signaling combined with shRNAs against RB1 and TP53. However, the resulting RP xenografts lacked important characteristics of SCLC. Unlike SCLC, these tumors proliferated slowly and did not metastasize, and although small subpopulations expressed MYC or MYCL, none expressed NEUROD1.

MYC is frequently amplified or expressed at high levels in SCLC, and here, the authors have tested whether inducible expression of MYC could increase the resemblance of their hPSC-derived NE tumors to SCLC. These RPM cells (or RPM T58A with stabilized cMYC) engrafted more consistently and grew more rapidly than RP cells, and unlike RP cells, formed liver metastases when injected into the renal capsule. Gene expression analyses reveled that RPM tumor subpopulations expressed NEUROD1, ASCL1 and/or YAP1.

The hPSC-derived RPM model is a major advance over the previous RP model. This may become a powerful tool for understanding SCLC tumorigenesis and progression and for discovering gene dependencies and molecular targets for novel therapies. However, the specific role of cMYC in this model needs to be clarified.

Recommended Revision:

cMYC can drive proliferation, tumorigenesis or apoptosis in a variety of lineages depending on concurrent mutations. For example, in the Park et al., study, normal human prostate cells could be reprogrammed to form adenocarcinoma-like tumors by activation of cMYC and AKT alone, without manipulation of TP53 or RB1. In their previous manuscript, the authors carefully showed the role of each molecular manipulation in NE tumorigenesis. DAPT was required for NE differentiation of LPs to PNECs, shRB1 was required for expansion of the PNECs, and shTP53 was required for xenograft formation. cMYC expression could influence

each of these steps, and importantly, could render some steps dispensable. For example, shRB1 was previously necessary to expand the DAPT-induced PNECs, as neither shTP53 nor activation of KRAS or EGFR had no effect on this population, but perhaps cMYC overexpression could expand PNECs even in the presence of pRB, or even induce LPs to become PNECs without DAPT. Similarly, both shRB1 and shTP53 were necessary for xenograft formation, but maybe not if cMYC is overexpressed. If a molecular hallmark of SCLC, such as loss of RB1 or TP53, has become dispensable with the addition of cMYC, this information is critically important in interpreting this as a model of SCLC tumorigenesis.

To interpret the role of cMYC expression in hPSC-derived RPM tumors, we need to know what this manipulation does without manipulation of pRB, p53 or NOTCH, alone or in combination. There are 7 relevant combinations that should be presented in this manuscript: (1) cMYC alone in LPs, (2) cMYC + DAPT, (3) cMYC + shRB1, (4) cMYC + DAPT + shRB1, (5) cMYC + shTP53, (6) cMYC + DAPT + shTP53, and (7) cMYC + shRB1 + shTP53. Wild-type cMYC is sufficient; further exploration with the T58A mutant would not be necessary.

Please present the effects of these combinations on LP differentiation to PNECs, expansion of PNECs as well as other lung cells, xenograft formation and histology, and xenograft growth rate and capacity for metastasis. If this could be clarified experimentally, and the results discussed in the context of other similar approaches such as the Park et al., paper, this study would be a major addition to the field.

https://doi.org/10.7554/eLife.93170.2.sa2

Reviewer #3 (Public review):

This revision and the accompanying rebuttal indicates the authors want to publish their studies without providing several of the reviewer requested additional experiments (such as determining the impact of other Myc family members on metastatic behavior and expression characteristics compared to overexpression of c-Myc), and determining whether the tumors were responsive or not to standard clinically used therapies. Their argument is the author team has moved on to other endeavors, it is important to communicate their findings to the research field, and they have indicated these issues in the Discussion. All of these things are reasonable. However, there two things that would help. The first is to have the authors clearly state in the Discussion section "Limitations of the current study" and then list these out. In the current format the indication that the authors recognize the "limitations" is not clearly stated. An example - of such a limitation is how well their model now provides a human SCLC like tumor that metastasizes. We know that in patients SCLC is widely metastatic, but in SCLC patient derived xenografts with subcutaneous injection that is not seen, so if their model now generated widely metastatic behavior like that seen in patients, this report and the associated resources would be a significant advance to the field. However, their data shows that using their model the subcutaneous tumors don't metastasize, and even with renal capsule models metastases are not common and do not go to important sites (e.g. brain). Second, a major reason for publishing this paper is that their model system would be available as a resource for the field to study. However, I could not find in the paper or the Methods section any statement as to the availability of this presumable important resource. If the resources will not be easily available in a format that others can readily study (e.g. with instructions on how to handle the cells which would seem to be more complicated than other patient derived SCLC models) then of course the value of this paper to the field as a whole is dramatically reduced. I would assume the authors want their model to be used by other investigators and thus a clear statement of model availability and how to routinely handle their model is important to include in their manuscript.

https://doi.org/10.7554/eLife.93170.2.sa1

Author response:

The following is the authors' response to the previous reviews.

Public Reviews:

Reviewer #1 (Public Review):

Summary:

The authors introduced their previous paper with the concise statement that "the relationships between lineage-specific attributes and genotypic differences of tumors are not understood" (Chen et al., JEM 2019, PMID: 30737256). For example, it is not clear why combined loss of RB1 and TP53 is required for tumorigenesis in SCLC or other aggressive neuroendocrine (NE) cancers, or why the oncogenic mutations in KRAS or EGFR that drive NSCLC tumorigenesis are found so infrequently in SCLC. This is the main question addressed by the previous and current papers.

One approach to this question is to identify a discrete set of genetic/biochemical manipulations that are sufficient to transform non-malignant human cells into SCLC-like tumors. One group reported the transformation of primary human bronchial epithelial cells into NE tumors through a complex lentiviral cocktail involving the inactivation of pRB and p53 and activation of AKT, cMYC, and BCL2 (PARCB) (Park et al., Science 2018, PMID: 30287662). The cocktail previously reported by Chen and colleagues to transform human pluripotent stem-cell (hPSC)-derived lung progenitors (LPs) into NE xenografts was more concise: DAPT to inactivate NOTCH signaling combined with shRNAs against RB1 and TP53. However, the resulting RP xenografts lacked important characteristics of SCLC. Unlike SCLC, these tumors proliferated slowly and did not metastasize, and although small subpopulations expressed MYC or MYCL, none expressed NEUROD1.

MYC is frequently amplified or expressed at high levels in SCLC, and here, the authors have tested whether inducible expression of MYC could increase the resemblance of their hPSC-derived NE tumors to SCLC. These RPM cells (or RPM T58A with stabilized cMYC) engrafted more consistently and grew more rapidly than RP cells, and unlike RP cells, formed liver metastases when injected into the renal capsule. Gene expression analyses revealed that RPM tumor subpopulations expressed NEUROD1, ASCL1, and/or YAP1.

The hPSC-derived RPM model is a major advance over the previous RP model. This may become a powerful tool for understanding SCLC tumorigenesis and progression and for discovering gene dependencies and molecular targets for novel therapies. However, the specific role of cMYC in this model needs to be clarified.

cMYC can drive proliferation, tumorigenesis, or apoptosis in a variety of lineages depending on concurrent mutations. For example, in the Park et al., study, normal human prostate cells could be reprogrammed to form adenocarcinoma-like tumors by activation of cMYC and AKT alone, without manipulation of TP53 or RB1. In their previous manuscript, the authors carefully showed the role of each molecular manipulation in NE tumorigenesis. DAPT was required for NE differentiation of LPs to PNECs, shRB1 was required for expansion of the PNECs, and shTP53 was required for xenograft formation. cMYC expression could influence each of these steps, and importantly, could render some steps dispensable. For example, shRB1 was previously necessary to expand the DAPT-induced PNECs, as neither shTP53 nor activation of KRAS or EGFR had no effect on this population, but perhaps cMYC overexpression could expand PNECs even in the presence of pRB, or even induce LPs to become PNECs without DAPT. Similarly, both shRB1 and shTP53 were necessary for xenograft formation, but maybe not if cMYC is overexpressed. If a molecular hallmark of SCLC, such as loss of RB1 or TP53, has become dispensable

> *with the addition of cMYC, this information is critically important in interpreting this as a model of SCLC tumorigenesis.*

The reviewer's suggestion may be possible; indeed, in a recent report from our group (Gardner EE, et al., Science 2024) we have shown, using genetically engineered mouse modeling coupled with lineage tracing, that the cMyc oncogene can selectively expand Ascl1+ PNECs in the lung.

We agree with the reviewer that not having a better understanding of the individual components necessary and/or sufficient to transform hESC-derived LPs is an important shortcoming of this current work. However, we would like to stress three important points about the comments: 1) tumors were reviewed and the histological diagnoses were certified by a practicing pulmonary pathologist at WCM (our co-author, C. Zhang); 2)the observed transcriptional programs were consistent with primary human SCLC; and 3) RB1-proficient SCLC is now recognized as a rare presentation of SCLC (Febrese-Aldana CA, et al., Clin. Can. Res. 2022. PMID: 35792876).

> *To interpret the role of cMYC expression in hPSC-derived RPM tumors, we need to know what this manipulation does without manipulation of pRB, p53, or NOTCH, alone or in combination. Seven relevant combinations should be presented in this manuscript: (1) cMYC alone in LPs, (2) cMYC + DAPT, (3) cMYC + shRB1, (4) cMYC + DAPT + shRB1, (5) cMYC + shTP53, (6) cMYC + DAPT + shTP53, and (7) cMYC + shRB1 + shTP53. Wildtype cMYC is sufficient; further exploration with the T58A mutant would not be necessary.*

We respectfully disagree that an interrogation of the differences between the phenotypes produced by wildtype and Myc(T58A) would not be informative. (Our view is confirmed by the second reviewer; see below.) It is well established that Myc gene or protein dosage can have profound effects on in vivo phenotypes (Murphy DJ, et al., Cancer Cell 2008. PMID: 19061836). The "RPM" model of variant SCLC developed by Trudy Oliver's lab relied on the conditional T58A point mutant of cMyc, originally made by Rob Wechsler-Reya. While we do not discuss the differences between Myc and Myc(T58A), it is nonetheless important to present our results with both the WT and mutant MYC constructs, as we are aware of others actively investigating differences between them in GEMM models of SCLC tumor development.

We agree with the reviewer about the virtues of trying to identify the effects of individual gene manipulations; indeed our original paper (Chen et al., J. Expt. Med. 2019), describing the RUES2derived model of SCLC did just that, carefully dissecting events required to transform LPs towards a SCLC-like state. The central purpose of the current study was to determine the effects of adding cMyc on the behavior of weakly tumorigenic SCLC-like cells cMyc. Presenting data with these two alleles to seek effects of different doses of MYC protein seems reasonable.

> *This reviewer considers that there should be a presentation of the effects of these combinations on LP differentiation to PNECs, expansion of PNECs as well as other lung cells, xenograft formation and histology, and xenograft growth rate and capacity for metastasis. If this could be clarified experimentally, and the results discussed in the context of other similar approaches such as the Park et al., paper, this study would be a major addition to the field.*
>
> ***Reviewer #2 (Public Review):***
>
> *Summary:*
>
> *Chen et al use human embryonic stem cells (ESCs) to determine the impact of wildtype MYC and a point mutant stable form of MYC (MYC-T58A) in the transformation of induced*

pulmonary neuroendocrine cells (PNEC) in the context of RB1/P53 (RP) loss (tumor suppressors that are nearly universally lost in small cell lung cancer (SCLC)). Upon transplant into immune-deficient mice, they find that RP-MYC and RP-MYC-T58A cells grow more rapidly, and are more likely to be metastatic when transplanted into the kidney capsule, than RP controls. Through single-cell RNA sequencing and immunostaining approaches, they find that these RPM tumors and their metastases express NEUROD1, which is a transcription factor whose expression marks a distinct molecular state of SCLC. While MYC is already known to promote aggressive NEUROD1+ SCLC in other models, these data demonstrate its capacity in a human setting that provides a rationale for further use of the ESC-based model going forward. Overall, these findings provide a minor advance over the previous characterization of this ESC-based model of SCLC published in Chen et al, J Exp Med, 2019.

We consider the findings more than a “minor” advance in the development of the model, since any useful model for SCLC would need to form aggressive and metastatic tumors.

The major conclusion of the paper is generally well supported, but some minor conclusions are inadequate and require important controls and more careful analysis.

Strengths:

(1) Both MYC and MYC-T58A yield similar results when RP-MYC and RP-MYCT58A PNEC ESCs are injected subcutaneously, or into the renal capsule, of immune-deficient mice, leading to the conclusion that MYC promotes faster growth and more metastases than RP controls.

(2) Consistent with numerous prior studies in mice with a neuroendocrine (NE) cell of origin (Mollaoglu et al, Cancer Cell, 2017; Ireland et al, Cancer Cell, 2020; Olsen et al, Genes Dev, 2021), MYC appears sufficient in the context of RB/P53 loss to induce the NEUROD1 state. Prior studies also show that MYC can convert human ASCL1+ neuroendocrine SCLC cell lines to a NEUROD1 state (Patel et al, Sci Advances, 2021); this study for the first time demonstrates that RB/P53/MYC from a human neuroendocrine cell of origin is sufficient to transform a NE state to aggressive NEUROD1+ SCLC. This finding provides a solid rationale for using the human ESC system to better understand the function of human oncogenes and tumor suppressors from a neuroendocrine origin.

Weaknesses:

(1) There is a major concern about the conclusion that MYC "yields a larger neuroendocrine compartment" related to Figures 4C and 4G, which is inadequately supported and likely inaccurate. There is overwhelming published data that while MYC can promote NEUROD1, it also tends to correlate with reduced ASCL1 and reduced NE fate (Mollaoglu et al, Cancer Cell, 2017; Zhang et al, TLCR, 2018; Ireland et al, Cancer Cell, 2020; Patel et al, Sci Advances, 2021). Most importantly, there is a lack of in vivo RP tumor controls to make the proper comparison to judge MYC's impact on neuroendocrine identity. RPM tumors are largely neuroendocrine compared to in vitro conditions, but since RP control tumors (in vivo) are missing, it is impossible to determine whether MYC promotes more or less neuroendocrine fate than RP controls. It is not appropriate to compare RPM tumors to in vitro RP cells when it comes to cell fate. Upon inspection of the sample identity in S1B, the fibroblast and basal-like cells appear to only grow in vitro and are not well represented in vivo; it is, therefore, unclear whether these are transformed or even lack RB/P53 or express MYC. Indeed, a close inspection of Figure S1B shows that RPM tumor cells have little ASCL1 expression, consistent with lower NE fate than expected in control RP tumors.

We would like to clarify two points related to the conclusions that we draw about MYC's ability to promote an increase in the neuroendocrine fraction in hESC-derived cultures: 1) The comparisons in Figures 4C were made between cells isolated in culture following the standard 50 day differentiation protocol, where, following generation of LPs around day 25, MYC was added to the other factors previously shown to enrich for a PNEC phenotype (shRB1, shTP53, and DAPT). Therefore, the argument that MYC increased the frequency of "neuroendocrine cells" (which we define by a gene expression signature) is a reasonable conclusion in the system we are using; and 2) following injection of these cells into immunocompromised mice, an ASCL1-low / NEUROD1-high presentation is noted (Supplemental Figures 1F-G). In the few metastases that we were able use to sequence bulk RNA, there is an even more pronounced increase in expression of NEUROD1 with a decrease in ASCL1.

Some confusion may have arisen from our previous characterization of neuroendocrine (NE) cells using either ASCL1 or NEUROD1 as markers. To clarify, we have now designated cells positive for ASCL1 as classical NE cells and those positive for NEUROD1 as the NE variant. According to this revised classification, our findings indicate that MYC expression leads to an increase in the NEUROD1+ NE variant and a decrease in ASCL1+ classical NE cells. This adjustment has been reflected on the results section titled, "Inoculation of the renal capsule facilitates metastasis of the RUES2-derived RPM tumors" of the manuscript.

From the limited samples in hand, we compared the expression of ASCL1 and NEUROD1 in the weakly tumorigenic hESC RP cells after successful primary engraftment into immunocompromised mice. As expected, the RP tumors were distinguished by the lack of expression of NEUROD1, compared to levels observed in the RPM tumors.

> *In addition, since MYC appears to require Notch signaling to induce NE fate (cf Ireland et al), the presence of DAPT in culture could enrich for NE fate despite MYC's presence. It's important to clarify in the legend of Fig 4A which samples are used in the scRNA-seq data and whether they were derived from in vitro or in vivo conditions (as such, Supplementary Figure S1B should be provided in the main figure). Given their conclusion is confusing and challenges robustly supported data in other models, it is critical to resolve this issue properly. I suspect when properly resolved, MYC actually consistently does reduce NE fate compared to RP controls, even though tumors are still relatively NE compared to completely distinct cellular identities such as fibroblasts.*

We have clarified the source of tumor sequencing data and the platform (single cell or bulk) in Figure 4 and Supplemental Figure 1. To reiterate – the RNA sequencing results from paired metastatic and primary tumors from the RPM model are derived from bulk RNA; the single cell RNA data in RP or RPM datasets are from cells in culture. These distinctions are clarified in the legend to Supplemental Figure 1.

> *(2) The rigor of the conclusions in Figure 1 would be strengthened by comparing an equivalent number of RP animals in the renal capsule assay, which is n = 6 compared to n = 11-14 in the MYC conditions.*

As we did not perform a power calculation to determine a sample size required to draw a level of statistical significance from our conclusions, this comment is not entirely accurate. Our statistical rigor was limited by the availability of samples from the RP tumor model.

> *(3) Statistical analysis is not provided for Figures 2A-2B, and while the results are compelling, may be strengthened by additional samples due to the variability observed.*

We acknowledge that the cohorts are relatively small but we have added statistical comparisons in Figure 2B.

> *(4a) Related to Figure 3, primary tumors and liver metastases from RPM or RPM-T58A-expressing cells express NEUROD1 by immunohistochemistry (IHC) but the putative negative controls (RP) are not shown, and there is no assessment of variability from tumor to tumor, ie, this is not quantified across multiple animals.*

The results of H&E and IF staining for ASCL1, NEUROD1, CGRP, and CD56 in negative control (RP tumors) are presented in the updated Figure 3F-G.

> *(4b) Relatedly, MYC has been shown to be able to push cells beyond NEUROD1 to a double-negative or YAP1+ state (Mollaoglu et al, Cancer Cell, 2017; Ireland et al, Cancer Cell, 2020), but the authors do not assess subtype markers by IHC. They do show subtype markers by mRNA levels in Fig 4B, and since there is expression of ASCL1, and potentially expression of YAP1 and POU2F3, it would be valuable to examine the protein levels by IHC in control RP vs. RPM samples.*

YAP1 positive SCLC is still somewhat controversial, so it is not clear what value staining for YAP1 offers beyond showing the well-established markers, ASCL1 and NEUROD1.

> *(5) Given that MYC has been shown to function distinctly from MYCL in SCLC models, it would have raised the impact and value of the study if MYC was compared to MYCL or MYCL fusions in this context since generally, SCLC expresses a MYC family member. However, it is quite possible that the control RP cells do express MYCL, and as such, it would be useful to show.*

We now include Supplemental Figure S2 to illustrate four important points raised by this reviewer and others: 1) expression of MYC family members in the merged dataset (RP and RPM) is low or undetectable in the basal/fibroblast cultures; 2) MYC does have a weak correlation with EGFP in the neuroendocrine cluster when either WT MYC or T58A MYC is overexpressed; 3) MYCL and MYCN are detectable, but at low levels compared to CMYC; and 4) Expression of ASCL1 is anticorrelated with MYC expression across the merged single cell datasets using RP and RPM models.

> ***Reviewer #3 (Public Review):***
>
> *Summary:*
>
> *The authors continue their study of the experimental model of small cell lung cancer (SCLC) they created from human embryonic stem cells (hESCs) using a protocol for differentiating the hESCs into pulmonary lineages followed by NOTCH signaling inactivation with DAPT, and then knockdown of TP53 and RB1 (RP models) with DOX inducible shRNAs. To this published model, they now add DOX-controlled activation of expression of a MYC or T58A MYC transgenes (RPM and RPMT58A models) and study the impact of this on xenograft tumor growth and metastases. Their major findings are that the addition of MYC increased dramatically subcutaneous tumor growth and also the growth of tumors implanted into the renal capsule. In addition, they only found liver and occasional lung metastases with renal capsule implantation. Molecular studies including scRNAseq showed that tumor lines with MYC or T58A MYC led surprisingly to more neuroendocrine differentiation, and (not surprisingly) that MYC expression was most highly correlated with NEUROD1 expression. Of interest, many of the hESCs with RPM/RPMT58A expressed ASCL1. Of note, even in the renal capsule RPM/RPMT58A models only 6/12 and 4/9 mice developed metastases (mainly liver with one lung*

> *metastasis) and a few mice of each type did not even develop a renal sub capsule tumor. The authors start their Discussion by concluding: " In this report, we show that the addition of an efficiently expressed transgene encoding normal or mutant human cMYC can convert weakly tumorigenic human PNEC cells, derived from a human ESC line and depleted of tumor suppressors RB1 and TP53, into highly malignant, metastatic SCLC-like cancers after implantation into the renal capsule of immunodeficient mice.".*
>
> *Strengths:*
>
> *The in vivo study of a human preclinical model of SCLC demonstrates the important role of c-Myc in the development of a malignant phenotype and metastases. Also the role of c-Myc in selecting for expression of NEUROD1 lineage oncogene expression.*
>
> *Weaknesses:*
>
> *There are no data on results from an orthotopic (pulmonary) implantation on generation of metastases; no comparative study of other myc family members (MYCL, MYCN); no indication of analyses of other common metastatic sites found in SCLC (e.g. brain, adrenal gland, lymph nodes, bone marrow); no studies of response to standard platin-etoposide doublet chemotherapy; no data on the status of NEUROD1 and ASCL1 expression in the individual metastatic lesions they identified.*

We have acknowledged from the outset that our study has significant limitations, as noted by this reviewer, and we explained in our initial letter of response why we need to present this limited, but still consequential, story at this time.

In particular, while we have attempted orthotopic transplantations of RPM tumor cells into NSG mice (by tail vein or intra-pulmonary injection, or intra-tracheal instillation of tumor cells), these methods were not successful in colonizing the lung. Additionally, we have compared the efficacy of platinum/etoposide to that of removing DOX in established RPM subcutaneous tumors, but we chose not to include these data as we lacked a chemotherapy responsive tumor model, and thus could not say with confidence that the chemotherapeutic agants were active and that the RPM models were truly resistant to standard SCLC chemotherapy. In a discussion about other metastatic sites, we have now included the following text:

“In animals administered DOX, histological examinations showed that approximately half developed metastases in distant organs, including the liver or lung (Figure 1D). No metastases were observed in the bone, brain, or lymph nodes. For a more detailed assessment, future studies could employ more sensitive imaging methods, such as luciferase imaging.”

> ***Recommendations for the authors:***
>
> ***Reviewer #2 (Recommendations For The Authors):***
>
> *Technical points related to Major Weakness #1:*
>
> *For Figure 4: Cells were enriched for EGFP-high cells only, under the hypothesis that cells with lower EGFP may have silenced expression of the integrated vector. Since EGFP is expressed only in the shRB1 construct, selection for high EGFP may inadvertently alter/exclude heterogeneity within the transformed population for the other transgenes (shP53, shMYC/MYC-T58A). Can authors include data to show the expression of MYC/MYC T58A in EGFP-high v -med v-low cells? MYC levels may alter the NEdifferentiation status of tumor cells.*

Please now refer to Supplemental Figure S2.

> *Related to the appropriateness of the methods for Figure 4C, the authors state, "We performed differential cluster abundance analysis after accounting for the fraction of cells that were EGFP+". If only EGFP+ cells were accounted for in the analysis for 4C, the majority of RP cells in the "Neuroendocrine differentiated" cluster would not be included in the analysis (according to EGFP expression in Fig S1A-B), and therefore inappropriately reduce NE identity compared to RPM samples that have higher levels of EGFP.*
>
> *There is no consideration or analysis of cell cycling/proliferation until after the conclusion is stated. Yet, increased proliferation of MYC-high vs MYC-low cultures would enhance selection for more tumors (termed "NE-diff") than non-tumors (basal/fibroblast) in 2D cultures.*
>
> *The expression of MYC itself isn't assessed for this analysis but assumed, and whether higher levels of MYC/MYC-T58A may be present in EGFP+ tumor cells that are in the NE-low populations isn't clear. Can MYC-T58A/HA also be included in the reference genome?*

We did not include an HA tag in our reference transcriptome. For [some] answers to this and other related questions, please refer to Supplemental Figure S2.

> ***Reviewer #3 (Recommendations For The Authors):***
>
> *(1) The experiments are all technically well done and clearly presented and represent a logical extension exploring the role of c-Myc in the hESC experimental model system.*

We appreciate this supportive comment!

> *(2) It is of great interest that both the initial RP model only forms "benign" tumors and that with the addition of a strong oncogene like c-myc, where expression is known to be associated with a very bad prognosis in SCLC, that while one gets tumor formation there are still occasional mice both for subcutaneous and renal capsule test sites that don't get tumors even with the injection of 500,000 RPM/RPMT58A cells. In addition, of the mice that do form tumors, only ~50% exhibit metastases from the renal sub-capsule site. The authors need to comment on this further in their Discussion. To me, this illustrates both how incredibly resistant/difficult it is to form metastases, thus indicating the need for other pathways to be activated to achieve such spread, and also represents an opportunity for further functional genomic tests using their preclinical model to systematically attack this problem. Obvious candidate genes are those recently identified in genetically engineered mouse models (GEMMs) related to neuronal behavior. In addition, we already know that full-fledged patient-derived SCLC when injected subcutaneously into immune-deprived mice don't exhibit metastases - thus, while the hESC RPM result is not surprising, it indicates to me the power of their model (logs less complicated genetically than a patient SCLC) to sort through a mechanism that would allow metastases to develop from subcutaneous sites. The authors can point these things out in their Discussion section to provide a "roadmap" for future research.*

Although we remain mindful of the relatively small cohorts we have studied, the thrust of Reviewer #3's comments is now included in the Discussion. And there is, of course, a lot more to do, and it has taken several years already to get to this point. Additional information about the prolonged gestation of this project and about the difficulties of doing more in the near future was described in our initial response to reviewers/Editor, included near the start of this letter.

> *(3) I will state the obvious that this paper would be much more valuable if they had compared and contrasted at least one of the myc family members (MYCL or MYCN) with*

> *the CMYC findings whatever the results would be. Most SCLC patients develop metastases, and most of their tumors don't express high levels of CMYC (and often use MYCL). In any event, as the authors Discuss, this will be an important next stage to test.*

We have acknowledged and explained the limitations of the work in several ways. Further, we were unaware of the relationship between metastases and the expression of MYC and MYCL1 noted by the reviewer; we will look for confirmation of this association in any future studies, although we have not encountered it in current literature.

> *(4) Their assays for metastases involved looking for anatomically "gross" lesions. While that is fine, particularly given that the "gross" lesions they show in figures are actually pretty small, we still need to know if they performed straightforward autopsies on mice and looked for other well-known sites of metastases in SCLC patients besides liver and lung - namely lymph nodes, adrenal, bone marrow, and brain. I would guess these would probably not show metastatic growth but with the current report, we don't know if these were looked for or not. Again, while this could be a "negative" result, the paper's value would be increased by these simple data. Let's assume no metastases are seen, then the authors could further strengthen the case for the value of their hESC model in systematically exploring with functional genomics the requirements to achieve metastases to these other sites.*

We have included descriptions of what we found and didn't find at other potential sites of metastasis in the results section, with the following sentences:

"In animals administered DOX, histological examinations showed that approximately half developed metastases in distant organs, including the liver or lung (Figure 1D). No metastases were observed in the bone, brain, or lymph nodes. For a more detailed assessment, future studies could employ more sensitive imaging methods, such as luciferase imaging."

> *(5) Related to this, we have no idea if the mice that developed liver metastases (or the one mouse with lung metastasis) had more than one metastatic site. They will know this and should report it. Again, my guess is that these were isolated metastases in each mouse. Again, they can indicate the value of their model in searching for programs that would increase the number of the various organs.*

We appreciate the suggestion. We observed that one of the mice developed metastatic tumors in both the liver and lungs. This information has been incorporated into the Results section.

> *(6) While renal capsule implantation for testing growth and metastatic behavior is reasonable and based on substantial literature using this site for implantation of patient tumor specimens, what would have increased the value of the paper is knowing the results from orthotopic (lung implantation). Whatever the results were (they occurred or did not occur) they will be important to know. I understand the "future experiments" argument, but in reading the manuscript this jumped out at me as an obvious thing for the authors to try.*

We conducted orthotopic implantation several ways, including via intra-tracheal instillation of 0.5 million RP or RPM cells in PBS per mouse. However, none of the subjects (0/5 mice) developed tumor-like growths and the number of animals used was small. Further, this outcome could be attributed to biological or physical factors. For instance, the conducting airway is coated with secretory cells producing protective mucins and may not have retained the 0.5 million cells. This is one example that may have hindered effective colonization. Future adjustments, such as increasing the number of cells, embedding them in Matrigel, or

damaging the airway to denude secretory cells and trigger regeneration might alter the outcomes. These ideas might guide future work to strengthen the utility of the models.

> *(7) Another obvious piece of data that would have improved the value of this manuscript would be to know whether the RPM tumors responded to platin-etoposide chemotherapy. Such data was not presented in their first RP hESC notch inhibition paper (which we now know generated what the authors call "benign" tumors). While I realize chemotherapy responses represent other types of experiments, as the authors point out one of the main reasons they developed their new human model was for therapy testing. Two papers in and we are all still asking - does their model respond or not respond dramatically to platin-etoposide therapy? Whatever the results are they are a vital next step in considering the use of their model.*

Please see the comments above regarding our decision not to include data from a clinical trial that lacked appropriate controls.

> *(8) The finding of RPM cells that expressed NEUROD1, ASCL1, or both was interesting. From the way the data were presented, I don't have a clear idea which of these lineage oncogenes the metastatic lesions from ~11 different mice expressed. Whatever the result is it would be useful to know - all NEUROD1, some ASCL1, some mixed etc.*

Based on the bulk RNA-sequencing of a few metastatic sites (Figure 4H), what we can demonstrate is that all sites were NEUROD1 and expressed low or no detectable ASCL1.

> *(9) While several H&E histologic images were presented, even when I enlarged them to 400% I couldn't clearly see most of them. For future reference, I think it would be important to have several high-quality images of the RP, RPM, RPMT58A subcutaneous tumors, sub-renal capsule tumors, and liver and lung metastatic lesions. If there is heterogeneity in the primary tumors or the metastases it would be important to show this. The quality of the images they have in the pdf file is suboptimal. If they have already provided higher-quality images - great. If not, I think in the long run as people come back to this paper, it will help both the field and the authors to have really great images of their tumors and metastases.*

We have attempted to improve the quality of the embedded images. Digital resolution is a tradeoff with data size – higher resolution images are always available upon request, but may not be suitable for generation of figures in a manuscript viewed on-line.

https://doi.org/10.7554/eLife.93170.2.sa0